Specification Document for OC6 Phase II: Verification of an Advanced Soil-Structure Interaction Model for Offshore Wind Turbines

Roger Bergua, Amy Robertson, Jason Jonkman, and Andy Platt

National Renewable Energy Laboratory

NREL is a national laboratory of the U.S. Department of Energy
Office of Energy Efficiency & Renewable Energy
Operated by the Alliance for Sustainable Energy, LLC

This report is available at no cost from the National Renewable Energy Laboratory (NREL) at www.nrel.gov/publications.

Contract No. DE-AC36-08GO28308

Technical Report
NREL/TP-5000-79938
July 2021

Specification Document for OC6 Phase II: Verification of an Advanced Soil-Structure Interaction Model for Offshore Wind Turbines

Roger Bergua, Amy Robertson, Jason Jonkman, and Andy Platt

National Renewable Energy Laboratory

Suggested Citation
Bergua, Roger, Amy Robertson, Jason Jonkman, and Andy Platt. 2021. *Specification Document for OC6 Phase II: Verification of an Advanced Soil-Structure Interaction Model for Offshore Wind Turbines*. Golden, CO: National Renewable Energy Laboratory. NREL/TP-5000-79938. https://www.nrel.gov/docs/fy21osti/79938.pdf.

NREL is a national laboratory of the U.S. Department of Energy
Office of Energy Efficiency & Renewable Energy
Operated by the Alliance for Sustainable Energy, LLC

This report is available at no cost from the National Renewable Energy Laboratory (NREL) at www.nrel.gov/publications.

Contract No. DE-AC36-08GO28308

Technical Report
NREL/TP-5000-79938
July 2021

National Renewable Energy Laboratory
15013 Denver West Parkway
Golden, CO 80401
303-275-3000 • www.nrel.gov

NOTICE

This work was authored by the National Renewable Energy Laboratory, operated by Alliance for Sustainable Energy, LLC, for the U.S. Department of Energy (DOE) under Contract No. DE-AC36-08GO28308. Funding provided by the U.S. Department of Energy Office of Energy Efficiency and Renewable Energy Wind Energy Technologies Office. The views expressed herein do not necessarily represent the views of the DOE or the U.S. Government.

Cover Photos by Dennis Schroeder: (clockwise, left to right) NREL 51934, NREL 45897, NREL 42160, NREL 45891, NREL 48097, NREL 46526.

Acknowledgments

The authors would like to thank the Norwegian Geotechnical Institute for their work in the REDWIN project to develop the capability incorporated in OC6 Phase II, for providing the data to model the foundation, and for their general support. We would also like to thank the Norwegian University of Science and Technology for their support in developing the model for this project.

List of Acronyms

AF	apparent fixity
DLL	dynamic link library
DOF	degree of freedom
FE	finite element
FEA	finite element analysis
IEA	International Energy Agency
MSL	mean sea level
NTM	normal turbulence model
OC6	Offshore Code Comparison Collaboration, Continued, with Correlation, and uncertainty
OWT	offshore wind turbine
PDF	probability density function
PSD	power spectral density
RNA	rotor-nacelle assembly
RWT	reference wind turbine
WAS-XL	Wave And Soil support for eXtra Large monopiles

Table of Contents

1 Introduction 1
2 REDWIN Macro-element Foundation Models 2
2.1 REDWIN Macro-element Model 2 2
2.2 Using REDWIN DLLs with OpenFAST (and Other Codes) 5
3 Model Definition 7
3.1 Coordinate System 7
3.2 Tower and Monopile 7
3.3 Soil-Structure Interaction 10
3.3.1 REDWIN Macro-element Model 2 10
3.3.2 Apparent Fixity Method 12
3.3.3 Improved Apparent Fixity Method 15
3.3.4 Distributed Springs: *p-y* Method 17
3.4 Rotor-Nacelle Assembly 18
4 Load Cases 20
5 Outputs 24
References 27
Appendix A. Load-displacement curves at seabed 29
Appendix B. Nonlinear *p-y* curves along the monopile 37
Appendix C. Soil-structure interaction damping 48
Appendix D. Externally applied loads 53

List of Figures

Figure 1. Illustration of the offshore wind turbine (left) and macro-element approach (right) 2
Figure 2. Nonlinear hysteretic pile foundation behavior 3
Figure 3. Loading conditions applied in the FEA to determine the load-displacement curves at seabed for REDWIN model 2: (a) overturning moment, (b) horizontal force 4
Figure 4. Global coordinate system 7
Figure 5. Schematic representation of the tower and monopile 9
Figure 6. Load-displacement curves at the seabed for REDWIN model 2: overturning moment 11
Figure 7. Load-displacement curves at the seabed for REDWIN model 2: horizontal force 11
Figure 8. FE model in Plaxis3D used by NGI 12
Figure 9. Schematic representation of the flexible foundation modeled by means of one beam using the AF method 12
Figure 10. Schematic representation of the flexible foundation modeled by means of two beams using the improved apparent fixity method 16
Figure 11. Nonlinear *p-y* relationship at different pile depths (z) 17
Figure 12. Schematic representation of the lumped springs along the monopile; L = 0.75 m 18
Figure C-1. Free-decay test for the REDWIN macro-element model and the equivalent elastic stiffness matrix at the seabed 48
Figure C-2. Illustrative plot of a free-decay test and the relationship between the amplitude at instant *t* and 3 periods away (n = 3) 49
Figure C-3. Global damping ratio for the first fore-aft bending mode for the REDWIN macro-element model and the equivalent elastic stiffness matrix at the seabed 50
Figure C-4. Force-displacement (left) and bending-rotation (right) relationships for the free-decay test at the seabed location 51
Figure C-5. Zoom-in of Figure C-4 with the equivalent stiffness denoted with a dashed black line for the force-displacement (left) and bending-rotation (right) relationships at the seabed 51
Figure D-1. Probability density function of rotor speed in LC 3.1 53
Figure D-2. Power spectral density of the fore-aft force at the yaw bearing for LC 3.1 54
Figure D-3. Probability density function of rotor speed in LC 3.2 54
Figure D-4. Power spectral density of the fore-aft force at the yaw bearing for LC 3.2 55
Figure D-5. Comparison of the power spectral density of the fore-aft force at the yaw bearing between LC 3.1 and LC 3.2 56

List of Tables

Table 1. Tower and Monopile Dimensions 8
Table 2. Tower and Monopile Material Properties 8
Table 3. Approximate Eigenfrequencies up to 2 Hz for the System Clamped at the Seabed 9
Table 4. Apparent Fixity Method Depending on the Beam Theory Used 15
Table 5. Improved Apparent Fixity Method 17
Table 6. RNA Mass Properties 18
Table 7. Prescribed Settings for Marine Conditions 21
Table 8. OC6 Phase II Load Case Simulations 23
Table 9. Output Format for LC 1.X, LC 3.X, LC 4.X, and LC 5.X 24
Table 10. Output Format for LC 2.X: Eigenfrequencies and Damping 26
Table 11. Output Format for LC 2.X: Mode Shapes 26
Table A-1. Horizontal Displacement and Rotation at Seabed for a Given Overturning Moment 29
Table A-2. Horizontal Displacement and Rotation at Seabed for a Given Horizontal Force 33
Table B-1. *p-y* Curves Along the Monopile 37
Table D-1. Main Excitations in the Externally Applied Loads for LC 3.1 53
Table D-2. Main Excitations in the Externally Applied Loads for LC 3.2 55

1 Introduction

The Norwegian Geotechnical Institute (NGI) has developed a new macro-element model (NGI 2018) that accounts for the soil-structure interaction in offshore wind turbines. This development was part of the REDWIN (REDucing cost of offshore WINd by integrated structural and geotechnical design) project (Page et al. 2018). The focus of Phase II of the Offshore Code Comparison Collaboration, Continued with Correlation and unCertainty (OC6) project was to integrate REDWIN's new soil-structure modeling capability into the coupled modeling tools that are used to design fixed-bottom offshore wind systems. The integration was then verified through a series of load cases using an example monopile-based offshore wind system examined within the WAS-XL project (Velarde and Bachynski 2017).

This document provides the details needed to model the system examined in OC6 Phase II using the new REDWIN modeling approach as well as other standard modeling approaches, including apparent fixity (AF), distributed springs, and coupled springs.

All simulation work related to this project will be made available in the near future on the Department of Energy's Data Archive in Portal (DAP) at https://a2e.energy.gov/projects/oc6.

2 REDWIN Macro-element Foundation Models

Three soil-foundations models were developed as part of the REDWIN project (NGI 2018). The models cover the most common foundation types for offshore wind turbines (OWTs) and are intended to be used in integrated time-domain simulation tools, where the wind turbine structure itself is the main focus of the analysis. The models were written in Fortran and compiled as dynamic link libraries (DLLs) in a Windows environment or through a shared object in a Linux environment.

REDWIN model 1 was developed primarily for piles that are intended to be analyzed by the traditional *p-y* approach. It can be used to model the distributed soil response along a monopile structure, a piled jacket, or the lumped response of a caisson foundation. REDWIN model 2 is intended to be used in monopile foundations by a single macro-element located at the seabed. The third model, REDWIN model 3, is a macro-element developed for shallow foundations, such as gravity-based and caisson foundations (e.g., three or four buckets that support a jacket structure).

OC6 Phase II focuses on verifying implementation of the REDWIN capability in participant modeling tools by investigating model 2 to describe the response of a pile foundation supporting a monopile-based OWT. This modeling approach is summarized in Section 2.1, and some guidance on coupling the DLL is provided in Section 2.2.

2.1 REDWIN Macro-element Model 2

In REDWIN model 2, the macro-element reduces the foundation and surrounding soil to a set of linear and nonlinear force-displacement relationships in the six degrees of freedom (DOF) of the interface point (the seabed) separating the foundation and the rest of the structure.

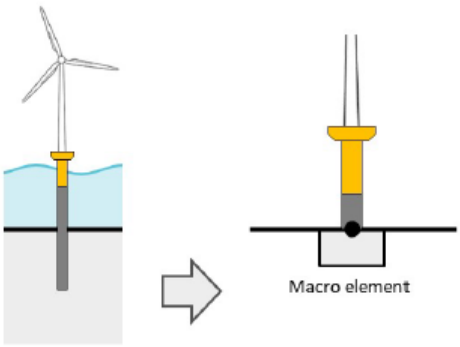

Figure 1. Illustration of the offshore wind turbine (left) and macro-element approach (right)

(Velarde and Bachynski 2017)

The macro-element communicates with the wind turbine model through a DLL or shared object. In each calculation step, the OWT simulation tool provides the displacements and rotations at the seabed to the foundation model, which transfers back the computed forces and moments. The soil-foundation model is solved following an explicit integration algorithm with corrector steps. The model also includes a substepping algorithm, which should help the convergence when the input displacement and/or rotation increment is large.

The macro-element allows an accurate and computationally efficient representation of the foundation stiffness and hysteretic damping (see Figure 2), crucial to performing reliable fatigue analysis. It is important to note that aerodynamic damping provides the highest contribution to the overall system damping; however, the importance of aerodynamic damping decreases in idling and wind-wave misalignment situations, increasing the importance of soil damping.

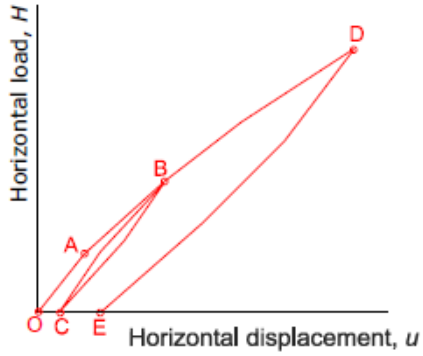

Figure 2. Nonlinear hysteretic pile foundation behavior

(Page et al. 2018)

As Figure 2 demonstrates, the macro-element model accounts for elasto-plastic behavior and provides different stiffness values during loading and unloading conditions. During the initial loading condition (points OAB in Figure 2), the foundation exhibits a nonlinear response due to the soil behavior. When the load acting on the foundation is released (lower trajectory from point B to C in Figure 2), the soil around the pile is unloaded. Initially the soil unloading is elastic, and the pile response is stiffer than prior to the unloading (slope of the right path below point B in Figure 2). As the magnitude of the load further decreases, plastic deformations are generated and the stiffness decreases (slope of the right path from point C in Figure 2). The next reloading condition is described by points CBD in Figure 2. The behavior is analogous to the one described for the trajectory OAB. The final unloading condition is described by points DE. A similar behavior as described for the trajectory between points BC is depicted. Note that the area of the loops described by these trajectories is indicative of the energy dissipated by the foundation. After the cycling loading described, there is one remaining displacement equal to the distance described by points OE. This remaining displacement after the cycling loading is due to the inherent plasticity of the system.

The sign convention for the REDWIN macro-element model is shown in Figure 4.

REDWIN model 2 requires two inputs from the user: (1) the coefficients of the elastic stiffness matrix at the seabed, and (2) two load-displacement curves at the seabed from nonlinear pushover analyses. In addition, a few numerical parameters must be specified. In OC6 Phase II, this information is supplied to the participants (see Section 3.3.1).

The coefficients for the elastic stiffness matrix should be obtained for an unloaded system considering the soil as linear elastic. For homogeneous profiles, the coefficients can be obtained from semiempirical formulas. For layered soil profiles or changes in stiffness with depth, the coefficients can be obtained from finite element analysis (FEA) of the structure and soil or by means of boundary element analysis.

The elastic stiffness matrix at the seabed should include all diagonal coefficients ($K_{11}, K_{22}, K_{33}, K_{44}, K_{55}, K_{66}$) and horizontal-rotational ($K_{15}, K_{24}, K_{42}, K_{51}$) coupling coefficients. The vertical (K_{33}) and torsional (K_{66}) directions are uncoupled from the other DOFs. See Eq. 1 for reference.

$$[K] = \begin{bmatrix} K_{11} & & & & K_{15} & \\ & K_{22} & & K_{24} & & \\ & & K_{33} & & & \\ & K_{42} & & K_{44} & & \\ K_{51} & & & & K_{55} & \\ & & & & & K_{66} \end{bmatrix} \quad (1)$$

The nonlinear load-displacement relationships at the interface point from the pushover analysis should be obtained from a soil model that represents the cyclic foundation response. From a practical point of view, this can be obtained from numerical analysis (i.e., quasi-static FEA) or experimentally.

Two analyses (or tests) are required to establish the load input curves (Figure 3): (1) a pushover analysis where a pure overturning moment (M) is applied at the pile head located at the seabed and the corresponding horizontal displacements (u_M) and rotations (θ_M) are obtained, and (2) a pushover analysis where a pure horizontal force (H) is applied at the pile head located at the seabed and the corresponding horizontal displacements (u_H) and rotations (θ_H) are obtained.

On the one side, the elastic stiffness matrix is used to predict the elastic foundation response. On the other side, the nonlinear load-displacement behavior is used to characterize the multisurface plasticity model. This last derivation is performed internally by the macro-element model (NGI 2018). Since the nonlinear load-displacement relationship does not include the vertical and torsional responses, these two DOFs will behave elastically.

It is important to note that the macro-element provides foundation stiffness and energy dissipation independently of the applied loading frequency.

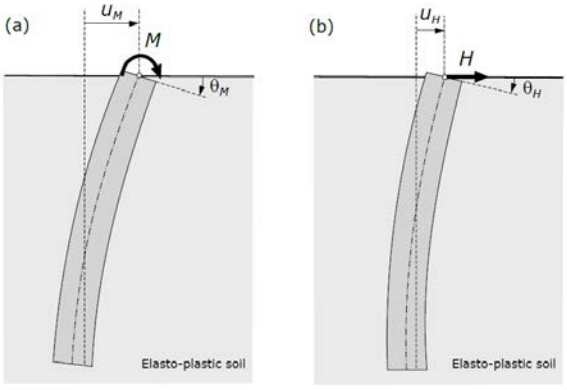

Figure 3. Loading conditions applied in the FEA to determine the load-displacement curves at seabed for REDWIN model 2: (a) overturning moment, (b) horizontal force

(Velarde and Bachynski 2017)

2.2 Using REDWIN DLLs with OpenFAST (and Other Codes)

Sample code is distributed with the REDWIN DLLs that illustrates two methods of linking the DLL into a code. The first method is a static linking at compile time, and the second method is dynamically loading the DLL at run time. When coupling the REDWIN DLL into other codes, such as OpenFAST, we recommend the dynamic linking method, *DLL not compiled together with simulation software*, outlined in Section A2 of the documentation for the DLL in Appendix A (Velarde and Bachynski 2017). This method allows for loading different model versions of the DLL as needed. This section is intended as a companion to the REDWIN documentation with additional lessons learned through incorporating the DLLs into the SoilDyn module in OpenFAST.

The SoilDyn module with example test cases and a driver will be released in an update to OpenFAST. This may provide additional hints not covered in this section to developers looking to incorporate REDWIN into their codes.

Some general tips for the linking are provided below.

DLL linking:

- The code provided with the REDWIN DLLs includes an example for dynamically linking (`testModel1_v2.f90`). This illustrates how to load and call the DLL.
- To avoid potential memory leaks, unload the library with the "*FreeLibrary*" function when ending the simulation (this is not given in the sample code).

```
USE kernel32, ONLY    : FreeLibrary
INTEGER(BOOL)        :: Success
Success = FreeLibrary( FileAddr ) ! True if success. FileAddr is address
                                  ! from call to load library call
```

- It is possible to use a single DLL for soil interactions at multiple points simultaneously. This requires keeping separate copies of all arguments passed to the DLL for each soil interaction point. In Fortran, this can be simplified with the use of a derived type as follows:

```
! Kind for eight-byte floating-point numbers
INTEGER, PARAMETER :: R8Ki = SELECTED_REAL_KIND( 14, 300 )

TYPE, PUBLIC :: REDWINdllType
    character(45)  :: PROPSFILE      !< Name of Properties file
    character(45)  :: LDISPFILE      !< Load-displacement curve file
    INTEGER        :: IDtask         !< Task identifier for DLL
    INTEGER        :: nErrorCode     !< number of returned error codes
    INTEGER,    DIMENSION(1:100)      :: ErrorCode  !< Array of error codes
    REAL(R8Ki), DIMENSION(1:100,1:200):: Props      !< model properties
    REAL(R8Ki), DIMENSION(1:12,1:100) :: StVar      !< state variables
    INTEGER,    DIMENSION(1:12,1:100) :: StVarPrint !< Unused placeholder
    REAL(R8Ki), DIMENSION(1:6)        :: Disp       !< Input displacements
    REAL(R8Ki), DIMENSION(1:6)        :: Force      !< Returned forces
    REAL(R8Ki), DIMENSION(1:6,1:6)    :: D          !< 6x6 stiffness matrix
  END TYPE REDWINdllType
```

- In dynamic linking of the DLL, the DLL may be in any convenient location; it does not need to be located with the simulation input data or the executable.

Arguments for the DLL:

See Table 1 in NGI (2018) for detailed descriptions of arguments passed to the DLL.

- The files `PROPSFILE` and `LDISPFILE` are used by the DLL. The path and file names cannot be longer than 45 characters. If the files are not found, a segmentation fault may occur. We recommend checking the existence of these files prior to calling the DLL.
- The `StVar` array contains the state information for a given soil interaction point. It may be possible to reset the interaction to a prior state by resetting this to a previous set of values, e.g., for corrector steps in time integration.
- The error codes returned in the `ErrorCode` array are specific to each DLL model. At present, there is no simple method of determining which DLL model has been loaded: none of the returned values appear to indicate this. This presents challenges in parsing the returned errors in the calling code.

Other notes:

- If the REDWIN DLL encounters an error, it will abort the program without returning any error codes.

3 Model Definition

In an effort to focus the verification work on the soil-structure interaction behavior, only the support structure was modeled, and a lumped mass and inertia was used to represent the rotor-nacelle assembly (RNA). The model definition and boundary conditions are presented in a way that allows repeatability by the participants involved in the project and external wind turbine engineers in the future.

3.1 Coordinate System

A global coordinate system (Germanischer 2010) is used for the description of the model and to output the results from the numerical models. The coordinate system is shown in Figure 4.

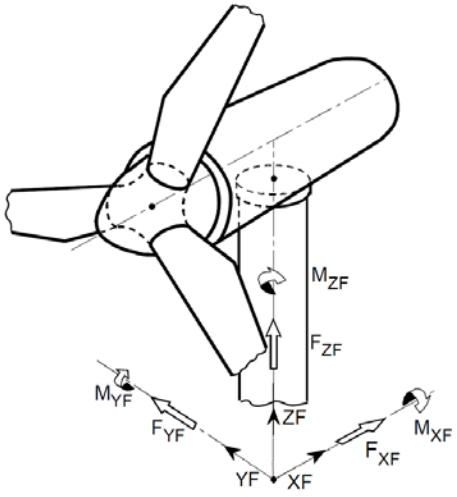

Figure 4. Global coordinate system

The x-axis of the global Cartesian coordinate system points downwind with respect to the main wind direction. The z-axis points upward (opposite gravity) and the y-axis forms a right-hand system.

3.2 Tower and Monopile

The tower used in OC6 Phase II is based on the offshore DTU 10-MW wind turbine design (Anaya-Lara 2020). The tower has a base outer diameter of 8.30 m with a thickness of 70 mm and a top outer diameter of 5.50 m with a thickness of 30 mm. The tower base begins at an elevation of 40 m above the seabed (10 m above the mean sea level [MSL]). The water depth considered is 30 m. The monopile extends from the tower base with an outer diameter of 9 m, a constant thickness of 110 mm, and a penetration depth of 45m, resulting in a length-to-diameter ratio of 5. The dimensions for the tower and monopile are included in Table 1, the material properties are presented in Table 2, and a schematic representation of the system is provided in Figure 5. The outer diameter and wall thickness varies linearly between the elevations given in Table 1.

The monopile design matches the one used in the WAS-XL (Wave And Soil support for eXtra Large monopiles) project (Velarde and Bachynski 2017). Funded by the Norwegian Research

Council, the WAS-XL project aims to reduce the uncertainties in large-diameter monopile design by improving hydrodynamic models for critical design loads and load history-consistent soil support modeling procedures.

Depending on the approach adopted by each participant, the structure below the seabed (denoted in grey in Figure 5) will have to be included or not. For example, the distributed springs approach presented in Section 3.3.4 needs this structural information.

Table 1. Tower and Monopile Dimensions

Location [-]	Elevation [m]	Outer Diameter ($\emptyset_{ext}$) [m]	Wall Thickness (t) [mm]
Yaw Bearing	145.63	5.50	30
	134.55	5.79	30
	124.04	6.07	35
	113.54	6.35	45
	103.03	6.63	50
	92.53	6.91	55
	82.02	7.19	60
	71.52	7.46	60
	61.01	7.74	65
	50.51	8.02	70
Tower Base	40.00	8.30	70
Monopile Top	40.00	9.00	110
Mean Sea Level	30.00	9.00	110
Seabed	0.00	9.00	110
Monopile Base	-45.00	9.00	110

Table 2. Tower and Monopile Material Properties

Parameter	Value
Young's modulus (E)	210 GPa
Shear modulus (G)	80.8 GPa
Density (ρ)	8,500 kg/m^3
Damping ratio (ζ_1) first bending mode	0.005
Damping ratio (ζ_2) second bending mode	0.01

The material density used for tower and monopile in Table 2 has been increased from the default value of 7,850 kg/m^3 to account for the mass of flanges, bolts, internal equipment, and paint; secondary structures; and other elements not otherwise accounted for in the wall thickness. The mass of the tower, according to the increased density, is 1,031,930 kg, and the mass of the

monopile from its connection with the tower base to the seabed is 1,044,536 kg. The eigenfrequencies of the system, considering the rotor-nacelle assembly (RNA) defined in Section 3.4 and assuming that the monopile is clamped at the seabed and there is no water in the system, are presented in Table 3. The structural damping considered for the first bending mode when the system is clamped at the seabed and the rigid RNA is placed atop of the tower is 0.5% critical damping. A damping of 1% critical damping is assumed for higher modes (e.g., second bending mode and torsion).

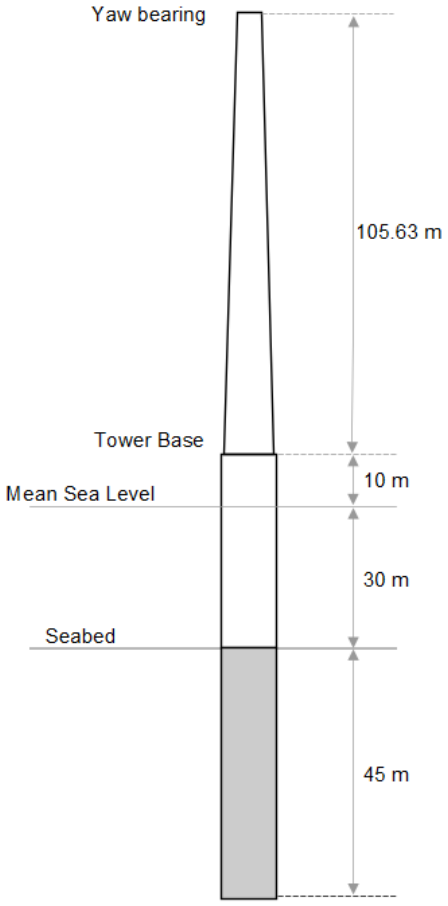

Figure 5. Schematic representation of the tower and monopile

Table 3. Approximate Eigenfrequencies up to 2 Hz for the System Clamped at the Seabed

Mode Shape	Eigenfrequency [Hz]
First fore/aft bending mode	0.28
First side/side bending mode	0.28
Second fore/aft bending mode	1.44
Second side/side bending mode	1.33
First torsional mode	1.27

3.3 Soil-Structure Interaction

This section provides the inputs used for the REDWIN macro-element model 2 explained in Section 2. In addition, three alternative ways to account for the soil-structure interaction are also presented: apparent fixity method (Sections 3.3.2 and 3.3.3), coupled springs approach (taking advantage of the stiffness matrix used in REDWIN [see Eq. 2 below]) and by means of distributed springs (Section 3.3.4). The focus of the project was to have participants couple the new REDWIN model to their offshore wind tools and verify it, but those who were not able to do this participated by modeling one of the alternative methods. The project leader, the National Renewable Energy Laboratory (NREL), modeled the system using different approaches to show the differences the REDWIN model provides.

3.3.1 REDWIN Macro-element Model 2

The information provided in this section corresponds to the model used in the WAS-XL project (Velarde and Bachynski 2017). The foundation model used in OC6 Phase II was calibrated by NGI (Sivasithamparam et al. 2020). It was not the intent of this project to derive the appropriate stiffness matrices for the REDWIN model, but to use the model already developed by WAS-XL.

The coefficients of the elastic stiffness matrix at the seabed used as an input for the REDWIN macro-element model 2 are provided in Eq. 2.

$$[K_{seabed\ 6x6}] = \begin{bmatrix} 6.336198E9 & 0 & 0 & 0 & -5.015421E10 & 0 \\ 0 & 6.336198E9 & 0 & 5.015421E10 & 0 & 0 \\ 0 & 0 & 1.119691E10 & 0 & 0 & 0 \\ 0 & 5.015421E10 & 0 & 8.111942E11 & 0 & 0 \\ -5.015421E10 & 0 & 0 & 0 & 8.111942E11 & 0 \\ 0 & 0 & 0 & 0 & 0 & 2.552673E11 \end{bmatrix} \quad (2)$$

The stiffness matrix in Eq. 2 accounts for the six degrees of freedom at the seabed and is expressed according to the coordinate system shown in Figure 4. The coefficients are expressed according to the international system of units (N, m, rad). As can be observed, the stiffness matrix is symmetric, which denotes reciprocity in the system.

The load-displacement curves used as input for the REDWIN macro-element model are shown in Figure 6 and Figure 7. The numerical values are available in Appendix A. These values were obtained from a nonlinear pushover analyses performed with a quasi-static FEA. The finite element (FE) model used is shown in Figure 8.

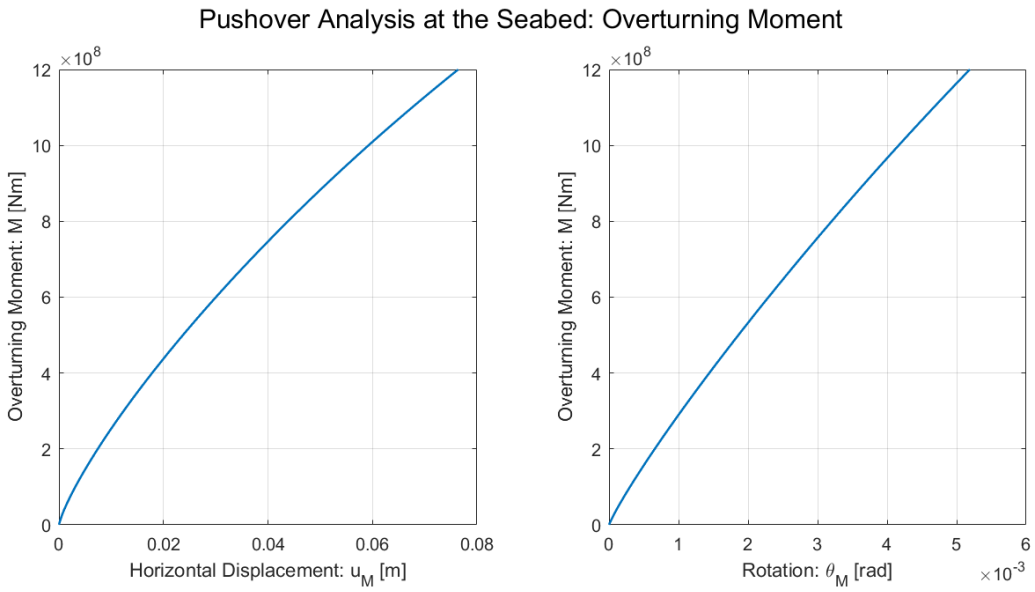

Figure 6. Load-displacement curves at the seabed for REDWIN model 2: overturning moment

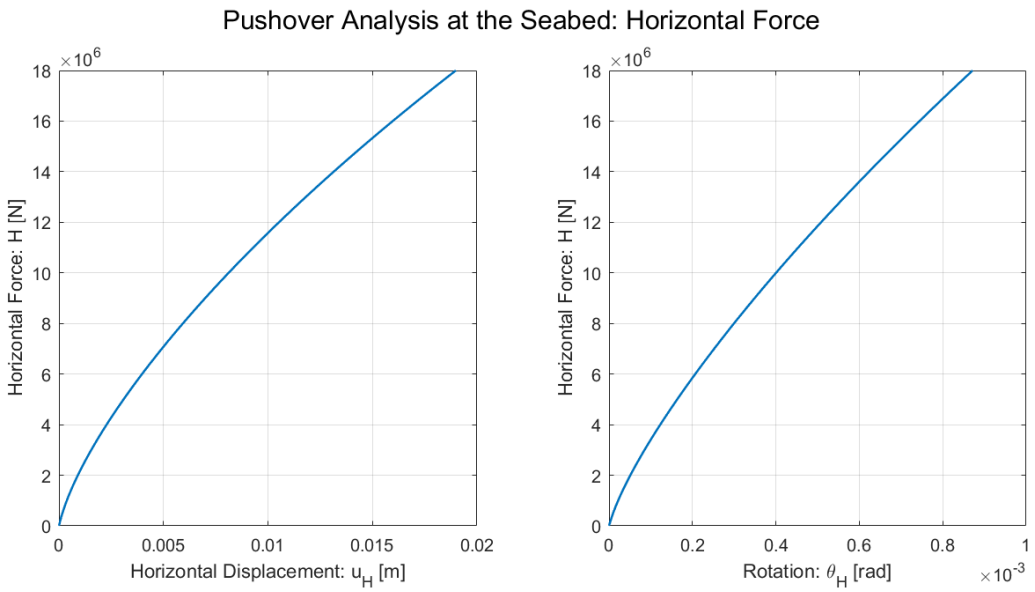

Figure 7. Load-displacement curves at the seabed for REDWIN model 2: horizontal force

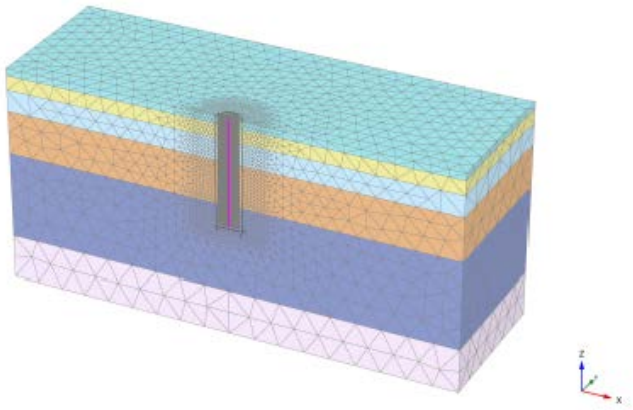

Figure 8. FE model in Plaxis3D used by NGI

(Sivasithamparam et al. 2020)

3.3.2 Apparent Fixity Method

The AF method assumes that the substructure is cantilevered at a depth that reproduces the same lateral displacement and rotation at the seabed as the true pile embedded in the soil. Figure 9 shows the schematic representation of the foundation using one beam with two nodes (N_1 and N_2). The lower node (N_1) has a clamp boundary condition.

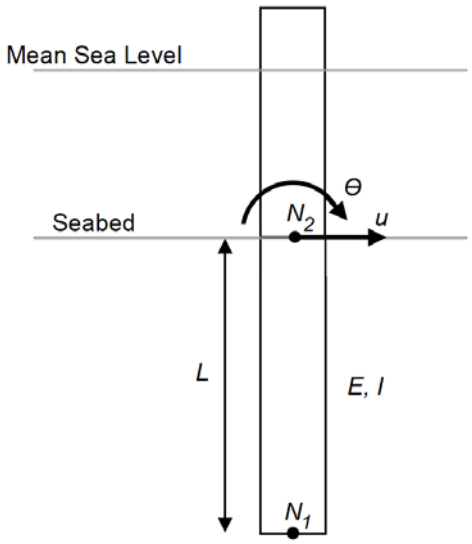

Figure 9. Schematic representation of the flexible foundation modeled by means of one beam using the AF method

3.3.2.1 Euler-Bernoulli Beam Theory

Eq. 3 shows the two-dimensional stiffness matrix for an axisymmetric cantilever beam for bending in one plane, neglecting the vertical and torsional DOFs.

$$[K] = \begin{bmatrix} K_{uu} & K_{u\theta} \\ K_{\theta u} & K_{\theta\theta} \end{bmatrix} = \begin{bmatrix} \frac{12EI}{L^3} & -\frac{6EI}{L^2} \\ -\frac{6EI}{L^2} & \frac{4EI}{L} \end{bmatrix} \quad (3)$$

The stiffness matrix used in Eq. 3 is based on the Euler-Bernoulli beam theory. EI corresponds to the bending stiffness, E is the Young's modulus, I is the second moment of area (also known as area moment of inertia), and L is the beam length. The stiffness matrix accounts for the horizontal stiffness (K_{uu}), the rotational stiffness ($K_{\theta\theta}$), and the cross-coupling stiffness between horizontal and rotational DOFs ($K_{u\theta} = K_{\theta u}$).

Eq. 4 shows the equivalent two-dimensional stiffness matrix at the seabed obtained from Eq. 2. This stiffness matrix accounts for the horizontal stiffness (coefficients K_{11} and K_{22} in Eq. 2), the rotational stiffness (coefficients K_{44} and K_{55} in Eq. 2) and the cross-coupling stiffness (coefficients K_{15} and K_{51} in Eq. 2).

$$[K_{seabed\ 2x2}] = \begin{bmatrix} 6.336198E9 & -5.015421E10 \\ -5.015421E10 & 8.111942E11 \end{bmatrix} \quad (4)$$

The coefficients in Eq. 4 are expressed according to the international system of units (N, m, rad).

It is common practice in the wind industry to only match the diagonal stiffness coefficients, providing two equations for the two unknowns, EI and L. But it is important to realize that without matching the off-diagonal coefficients (cross-coupling coefficients), the translational and rotational displacements at the seabed cannot be reproduced with accuracy.

To match both the diagonal and off-diagonal coefficients when using the Euler-Bernoulli beam theory, it is necessary to use more than one beam with different properties (Løken 2017). Although three equations (two diagonal coefficients and one off-diagonal coefficient) and three unknows could be considered in Eq. 3 (e.g., E, I, and L), the system of equations is linearly dependent because all three equations have EI (bending stiffness) at the numerator. Section 3.3.3 proposes an approach using more than one Euler-Bernoulli beam to match the diagonal and off-diagonal coefficients.

Therefore, in this section the properties of the Euler-Bernoulli beam (Eq. 3) will be tuned to match the diagonal coefficients of the stiffness matrix shown in Eq. 4, disregarding the off-diagonal coefficients.

In this case, the diameter and wall thickness of the beam was kept the same as for the monopile at the seabed. Accordingly, the second moment of area can be calculated as shown in Eq. 5.

$$I = \frac{\pi}{4}\left(\left(\frac{\emptyset_{ext}}{2}\right)^4 - \left(\frac{\emptyset_{int}}{2}\right)^4\right) = \frac{\pi}{4}\left(\left(\frac{9}{2}\right)^4 - \left(\frac{9-2*0.110}{2}\right)^4\right) = 30.355\ m^4 \quad (5)$$

Considering Eq. 5 and by solving Eq. 3 to match the diagonal coefficients of Eq. 4, the apparent fixity length and Young modulus obtained are: L = 19.60 m and E = 130.93E9 N/m^2.

3.3.2.2 Timoshenko Beam Theory

Many simulation tools in the wind industry use Timoshenko beam theory. For Timoshenko beam formulations, the shear correction factor (K_s) must be taken into account. Eq. 6 shows the two-dimensional stiffness matrix using the Timoshenko beam formulation for an axisymmetric cantilever beam for bending in one plane, neglecting the vertical and torsional DOFs.

$$[K] = \begin{bmatrix} K_{uu} & K_{u\theta} \\ K_{\theta u} & K_{\theta\theta} \end{bmatrix} = \begin{bmatrix} \frac{12EI}{L^3(1+K_s)} & -\frac{6EI}{L^2(1+K_s)} \\ -\frac{6EI}{L^2(1+K_s)} & \frac{(4+K_s)EI}{L(1+K_s)} \end{bmatrix} \quad (6)$$

Note that considering a null shear correction factor (K_S = 0) in Eq. 6, would return the stiffness matrix using the Euler-Bernoulli beam formulation shown in Eq. 3.

Unlike for the Euler-Bernoulli formulation, the equations for the diagonal and off-diagonal coefficients in Eq. 6 are linearly independent. Therefore, the system using one Timoshenko beam can match the diagonal and off-diagonal coefficients of the stiffness matrix.

The shear correction factor for a hollow circular cross-section can be determined by means of Eq. 7, according to Damiani et al. (2015).

$$K_s = \frac{12EI}{GA_sL^2} \quad (7)$$

Where G corresponds to the shear modulus, and A_s corresponds to the shear area along any axis in the cross-sectional plane passing through the center of the beam.

The shear modulus can be determined according to Eq. 8.

$$G = \frac{E}{2(1+\nu)} \quad (8)$$

where ν is the Poisson coefficient.

and the shear area, A_s, can be determined according to Eq. 9.

$$A_s = k * A \quad (9)$$

where A (Eq. 10) corresponds to the beam cross-sectional area, and *k* (Eq. 11) is a constant used to define the characteristic structure.

$$A = \pi\left(\left(\frac{\emptyset_{ext}}{2}\right)^2 - \left(\frac{\emptyset_{int}}{2}\right)^2\right) \quad (10)$$

$$k = \frac{6(1+v)^2\left(1+\left(\frac{\emptyset_{int}}{\emptyset_{ext}}\right)^2\right)^2}{\left(1+\left(\frac{\emptyset_{int}}{\emptyset_{ext}}\right)^2\right)^2(7+14v+8v^2)+4\left(\frac{\emptyset_{int}}{\emptyset_{ext}}\right)^2(5+10v+4v\text{^}2)} \quad (11)$$

In this case, the external diameter of the beam was kept the same as for the monopile at the seabed, and the unknows considered were the beam length (L), the Young's modulus (E), and the internal diameter ($Ø_{int}$). Having the internal diameter as an unknown requires checking that the solution for this parameter is in the range between 0 and the external diameter (feasible solution). Other strategies in terms of the unknows could also have been adopted to solve the system.

By solving Eq. 6 to match Eq. 4, the apparent fixity length, Young's modulus and beam internal diameter obtained are: L = 15.83 m, E = 41.07E9 N/m^2 and $Ø_{int}$ = 7.58 m.

Table 4 summarizes the parameters and equivalent stiffness at the seabed for the apparent fixity method.

As Table 4 shows, the Euler-Bernoulli beam approach only matches the diagonal coefficients, whereas the Timoshenko beam approach matches the diagonal and off-diagonal coefficients. In this case, the off-diagonal coefficient is a high value that plays an important role when trying to reproduce the correct behavior at the seabed. For simulation tools employing a Euler-Bernoulli beam formulation, the improved AF method detailed in Section 3.3.3 should be used.

Table 4. Apparent Fixity Method Depending on the Beam Theory Used

Approach	Beam Theory	Parameters	Equivalent Stiffness Matrix at the Seabed
AF method	Euler-Bernoulli	L = 19.60 m E = 130.93E9 N/m^2 $Ø_{ext}$ = 9 m $Ø_{int}$ = 8.78 m	K_{uu} = 6.34E9 N/m $K_{u\theta}$ = -6.21E10 N/rad $K_{\theta u}$ = -6.21E10 Nm/m $K_{\theta\theta}$ = 8.11E11 Nm/rad
	Timoshenko	L = 15.83 m E = 41.07E9 N/m^2 $Ø_{ext}$ = 9 m $Ø_{int}$ = 7.58 m ν = 0.3	K_{uu} = 6.34E9 N/m $K_{u\theta}$ = -5.02E10 N/rad $K_{\theta u}$ = -5.02E10 Nm/m $K_{\theta\theta}$ = 8.11E11 Nm/rad

3.3.3 Improved Apparent Fixity Method

As mentioned in Section 3.3.2.1, to match the diagonal and off-diagonal coefficients of the stiffness matrix using the Euler-Bernoulli beam theory, it is necessary to use, at least, two beams with different properties.

Figure 10 shows the schematic representation of the foundation using two beams with three nodes (N_1, N_2 and N_3). The upper beam is beam number two and the lower beam is beam number one. The lower node of beam one (N_1) has a clamp boundary condition.

Løken (2017) proposes to determine the properties of the two beams by means of the flexibility matrix at the seabed. The flexibility matrix is the inverse of the stiffness matrix, and it is indicative of the deflection or rotation for an applied unit of force or moment. The flexibility matrix at the seabed can be formulated, for a two-dimensional system, as shown in Eq. 12.

$$[K_{seabed\ 2x2}]^{-1} = \begin{bmatrix} \delta_{uu} & \delta_{u\theta} \\ \delta_{\theta u} & \delta_{\theta\theta} \end{bmatrix} \qquad (12)$$

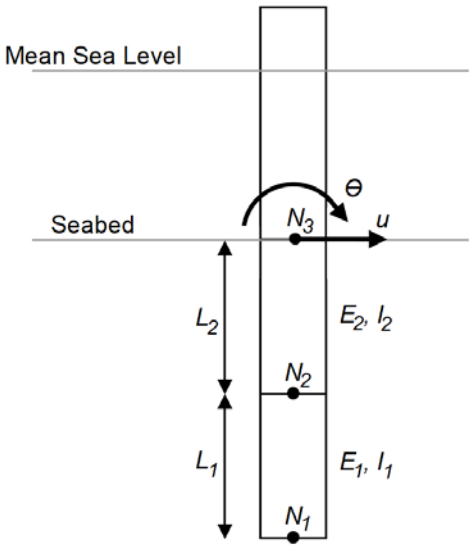

Figure 10. Schematic representation of the flexible foundation modeled by means of two beams using the improved apparent fixity method

where δ_{uu} is the horizontal displacement caused by a unitary horizontal force, $\delta_{u\theta}$ is the rotation caused by a unitary horizontal force, $\delta_{\theta u}$ is the horizontal displacement caused by a unitary overturning moment, and $\delta_{\theta\theta}$ is the rotation caused by a unitary overturning moment.

From the work done by Løken (2017), the next relationships can be established:

$$\delta_{uu} = \frac{1}{E_1 I_1}\left(\frac{L_1^3}{3} + L_1^2 L_2 + L_2^2 L1\right) + \frac{L_2^3}{3E_2 I_2} \qquad (13)$$

$$\delta_{u\theta} = \delta_{\theta u} = \frac{1}{E_1 I_1}\left(\frac{L_1^2}{2} + L_1 L_2\right) + \frac{L_2^2}{2E_2 I_2} \qquad (14)$$

$$\delta_{\theta\theta} = \frac{L_1}{E_1 L_1} + \frac{L_2}{E_2 L_2} \qquad (15)$$

There are different combinations of the parameters of the two beams that could provide the desired behavior at the seabed. In this case, the diameter and wall thickness of the two beams were kept the same as for the monopile at the seabed. Therefore, the second moment of area is the same as for the apparent fixity method described in Section 3.3.2.1 ($I_2 = I_1 = I$). In addition, an arbitrary value can be assigned to the length of the upper beam (e.g., $L_2 = 5$ m). This leaves the length of the lower beam (L_1) and the Young's modulus of the two beams (E_1 and E_2) as the three unknown parameters.

Table 5 summarizes the parameters and equivalent stiffness at the seabed for the improved apparent fixity method.

Table 5. Improved Apparent Fixity Method

Approach	Beam Theory	Parameters	Equivalent Stiffness Matrix at Seabed
Improved apparent fixity method	Euler-Bernoulli	L_1= 23.15 m E_1= 821.17E9 N/m^2 L_2= 5.00 m E_2= 110.89E9 N/m^2 $\emptyset_{ext}$ = 9 m $\emptyset_{int}$ = 8.78 m	K_{uu} = 6.34E9 N/m $K_{u\theta}$ = -5.02E10 N/rad $K_{\theta u}$ = -5.02E10 Nm/m $K_{\theta\theta}$ = 8.11E11 Nm/rad

3.3.4 Distributed Springs: *p-y* Method

The lateral load-deflection behavior along the monopile has been characterized by NGI (Sivasithamparam et al 2020) for the WAS-XL monopile by means of a series of *p-y* curves. The *p-y* curves are derived from 3D finite element analyses of the soil volume and the pile, which is more accurate than using the API semiempirical functions. In total there are 61 *p-y* curves defined every 0.75 m along the monopile. Each *p-y* curve is defined by 22 points. The numerical values of the *p-y* curves are available in Appendix B.

It is important to note that *p* is the resultant soil resistance force per unit length of pile that occurs when the unit length of pile is displaced a lateral distance, *y*, into the soil. Figure 11 shows, for illustrative purposes, the *p-y* relationship at different pile depths. As can be observed, the relationship between the lateral soil resistance, *p*, and the lateral pile displacement, *y*, is nonlinear and varies along the pile depth.

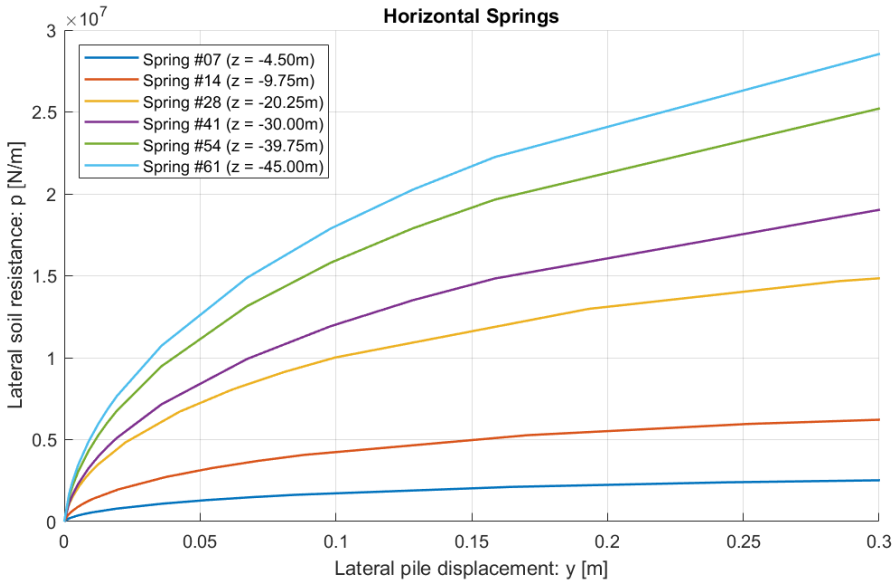

Figure 11. Nonlinear *p-y* relationship at different pile depths (z)

The relationship between the lateral soil resistance force per unit length, *p*, and the lateral pile displacement, *y*, can be considered as a distributed stiffness. It is possible to work with a lumped stiffness rather than a distributed stiffness by multiplying *p* by the part of pile length of interest.

This force-displacement relationship allows the soil-structure interaction (SSI) to be modeled using independent nonlinear springs. This process is illustrated in Figure 12.

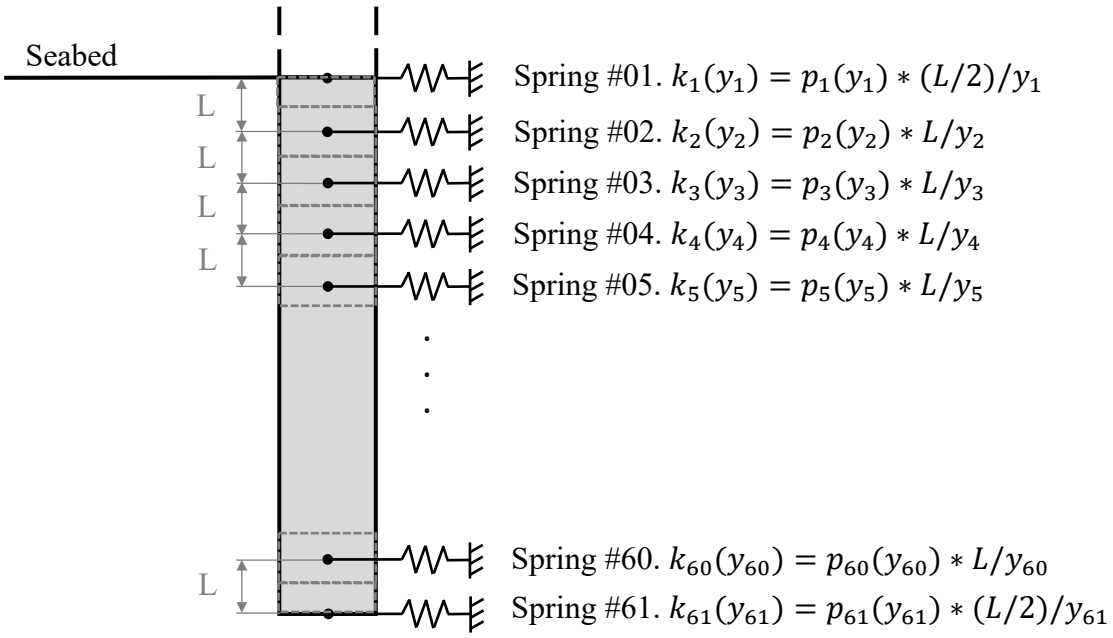

Figure 12. Schematic representation of the lumped springs along the monopile; L = 0.75 m

3.4 Rotor-Nacelle Assembly

The RNA is modeled as a lumped mass and inertia at the location indicated in Table 6, which uses the standard wind turbine convention of Figure 4. The properties used can be considered representative of the ones from the IEA-10.0-198-RWT. This RWT is a direct-drive design developed as part of International Energy Agency (IEA) Wind Task 37 (Bortolotti et al. 2019).

Table 6. RNA Mass Properties

CM stands for center of mass and I for moments of inertia

Parameter	Value	Description
Mass	839,741 kg	Total tower-top mass
CM_x	-5.80 m	Center of mass in X direction from yaw bearing
CM_y	0 m	Center of mass in Y direction from yaw bearing
CM_z	3.19 m	Center of mass in Z direction from yaw bearing
I_{xx}	1.84E8 kg m^2	Moment of inertia around X axis at the center of mass
I_{yy}	9.61E7 kg m^2	Moment of inertia around Y axis at the center of mass
I_{zz}	1.06E8 kg m^2	Moment of inertia around Z axis at the center of mass
$I_{xy} = I_{yx}$	0 kg m^2	XY product of inertia at the center of mass
$I_{xz} = I_{zx}$	-7.11E6 kg m^2	XZ product of inertia at the center of mass
$I_{yz} = I_{zy}$	0 kg m^2	YZ product of inertia at the center of mass

For reference, the moment of inertia tensor for a point-mass is given by Eq. 16.

$$[I] = \begin{bmatrix} I_{xx} & I_{xy} & I_{xz} \\ I_{yx} & I_{yy} & I_{yz} \\ I_{zx} & I_{zy} & I_{zz} \end{bmatrix} = \begin{bmatrix} m(y^2 + z^2) & -mxy & -mxz \\ -myx & m(x^2 + z^2) & -myz \\ -mzx & -mzy & m(x^2 + y^2) \end{bmatrix} \quad (16)$$

On the one hand, the products of inertia I_{xy} and I_{yz} equal to zero reported in Table 6 denote the symmetry about the XZ plane in the system. On the other hand, the product of inertia I_{xz} being different than 0 denotes that the X and Z principal axes of inertia have a different orientation than the global coordinate system (Figure 4).

4 Load Cases

Table 8 provides a summary of the simulations performed, which includes static simulations (1.X), eigen-analyses (2.X), wind-only simulations (3.X), wave-only simulations (4.X), and combined wind/wave simulations (5.X).

LC 1.1 and LC 1.2 focus on ensuring that the structural model has been implemented correctly by examining the static loads and deflections of the system with gravity as the only external loading. LC 1.3 includes one horizontal force (F_x = 1,500 kN) at the yaw bearing (tower top) representative of the thrust force at rated wind speed for the IEA-10.0-198-RWT (Bortolotti et al. 2019).

LC 2.X furthers the examination of the structural model by assessing the system eigenfrequencies, damping values, and mode shapes for three configurations, including/excluding the foundation and also including/excluding still water. The eigen-properties should be obtained around the static equilibrium and consider the gravity acceleration over the system. Moreover, the eigenfrequency provided should correspond to the undamped natural frequency. The undamped natural frequency is related to the damped natural frequency, according to Eq. 17. However, the difference between frequencies is expected to be negligible due to the relatively small damping ratio in the system.

$$f_{damped} = f_{undamped} * \sqrt{1 - \zeta^2} \qquad (17)$$

The method for assessing the eigen-properties is up to the modeler and can be accomplished using a linearization methodology in the modeling tool, through a free-decay simulation, or through a broad-band wind or wave excitation.

In Appendix C, the SSI damping is characterized at different loading levels. The participants using one SSI method that does not include damping (e.g., apparent fixity, coupled springs, and distributed springs) can use the values reported in Appendix C to include the SSI damping in their numerical models. This SSI damping is important for LC 2.X (eigen analysis) and LC 3–5 (dynamic analysis).

LC 3–5 then focus on assessing the response loads and motions of the full monopile-based OWT when considering wind and wave loading separately, and then in combination. As mentioned in Section 3, the computational models account for the support structure and a lumped mass and inertia for the RNA. The wind loading for load cases 3 and 5 (see Table 8) is computed beforehand and will be applied as an external force by participants at the yaw bearing. NREL calculates the force using an aeroelastic model of the IEA-10.0-198-RWT with turbulent wind. The IEA-10.0-198-RWT is an IEC class IA (Bortolotti et al. 2019) wind turbine. Accordingly, the turbulent winds use the IEC Kaimal wind spectrum (IEC 2009) with turbulence according to the normal turbulence model (NTM) for Class A turbines. The wind shear power law exponent used is α = 0.14 (IEC 2009). The loads at the yaw bearing location are obtained using simulations that consider the structural components of the wind turbine (i.e., supporting structure, drivetrain, and blades) as rigid and do not account for gravity acceleration. In this way, the inertial and gravity loads are disregarded, and the loads can be considered externally applied.

The participants can then account for the gravity and inertia loading in their simulation tools and prescribe these time series of loads as non-follower loads applied at the yaw bearing location.

LC 3.X focuses on wind-only load cases. LC 3.1 considers a mean wind speed at hub height (V_{hub}) of 9.06 m/s. This wind speed is below the rated wind speed of 10.75 m/s for the IEA-10.0-198-RWT (Bortolotti et al. 2019). LC 3.2 examines the system response for a mean wind speed of 20.90 m/s. For LC 3.X, NREL will provide 4,000 s times series of loads to be applied at the yaw bearing location. See Appendix D for additional information. Participants should report 3,600 s of response time, to exclude initial transients. The simulation length is increased from the 600 s recommended in the IEC standard (IEC 2009) to get statistically comparable results between participants. These winds are also used in LC 5.X in combination with irregular waves (stochastic loading).

OC6 Phase II focused on the verification of the soil-structure interaction model and therefore used a simple modeling approach for the hydrodynamic forces. Table 7 provides the settings for the load cases that involve marine conditions to try to replicate the same input loading across participants and simulation tools.

Table 7. Prescribed Settings for Marine Conditions

Hydrodynamic Forces	Wave Kinematics	Seawater Density
Relative form of Morison equation (without corrections) Drag coefficient (C_D) = 1 Inertia coefficient (C_M) = 2	Linear (first order) waves No wave stretching No directional spreading	1,025 kg/m^3 (IEC 2009)

As stated in Table 7, the waves are generated using first-order (linear Airy) wave theory and the wave kinematics are only computed up to the mean sea level rather than the instantaneous water level (no wave stretching). The hydrodynamic loads are computed based on the relative form of the Morison equation. This formulation accounts for the distributed viscous-drag, fluid-inertia, and added-mass components. As can be observed in Eq. 17, the relative form of the Morison equation considers the relative motion between the fluid and the structure.

$$F = \frac{1}{2} \cdot C_D \cdot \rho \cdot D \cdot (u_w - u_s) \cdot |u_w - u_s| + C_M \cdot \rho \cdot \frac{\pi \cdot D^2}{4} \cdot \dot{u}_w - C_A \cdot \rho \cdot \frac{\pi \cdot D^2}{4} \cdot \dot{u}_s \qquad (17)$$

where F is the force per unit length on the cylinder, u_w is the fluid velocity, u_s is the structure velocity, $\dot{u}_w$ is the fluid acceleration, $\dot{u}_s$ is the structure acceleration, D is the cylinder outer diameter, ρ is the fluid density, C_D is the drag coefficient, C_M is the inertia coefficient, and C_A is the added mass coefficient ($C_A = C_M - 1$).

LC 4.X focuses on wave-only load cases. LC 4.1 analyzes the response of the system for a regular wave height (H) of 5.50 m and regular wave period (T) of 9.0 s. For this load case, each participant must account for the necessary pre-simulation time to ensure that the results are representative of the steady state at the beginning of the reported results. In addition, the results must be provided starting with the wave at the peak and decreasing in time. The output time series should have a length of 90 s (corresponding to 10 wave cycles). LC 4.2 studies the response of the system for a Pierson-Moskovitz wave spectrum with a significant wave height

(H_s) of 1.25 m and peak-spectral wave period (T_p) of 5.5 s. LC 4.3 is representative of a storm condition in the North Sea for a 30-m water depth site (Bachynski et al. 2019). LC 4.3 is based on a JONSWAP wave spectrum with H_s = 7.60 m, T_p = 8.6 s and peak-enhancement factor (γ) equal to 5 according to the IEC (2009). During this storm condition, the mean wind speed at hub height is 34.6 m/s. This mean wind speed is above the cut-out wind speed (25 m/s for the IEA-10.0-198-RWT [Bortolotti et al. 2019]). Therefore, the wind turbine is in idling conditions. For LC 4.2 and LC 4.3 the initial transient response should be disregarded. Participants are asked to supply a time series response (without transient data) of 3,600 s.

LC 5.X is representative of the environmental conditions of a 30-m water depth site at the Norwegian Continental Shelf (Katsikogiannis et al. 2019). LC 5.1 combines the wind conditions proposed in LC 3.1 with the Pierson-Moskowitz wave spectrum analyzed in LC 4.2. LC 5.2 combines the wind conditions proposed in LC 3.2 with a JONSWAP wave spectrum with H_s = 3.75 m, T_p = 7.5 s, and γ = 1.37. The peak-enhancement factor is calculated according to IEC (2009). For LC 5.X the initial transient response should be disregarded. The time series used to analyze the outputs in these load cases have a length of 3,600 s.

The simulated wave elevation for LC 4.2, LC 4.3, and LC 5.X is provided for those participants who can input the time series directly in their simulation tool.

It is important to note that the responses from load cases that involve wind (i.e., LC 3.X and LC 5.X) are used for verification purposes but cannot be considered representative of a real wind turbine in operating conditions due to the lack of aerodynamic damping in the models.

Table 8. OC6 Phase II Load Case Simulations

	Load Case	Enabled DOFs	Wind Conditions	Marine Conditions	Comparison Type
Static Analysis	1.1	Tower, substructure (clamp at seabed)	None	None	Static response
	1.2	Tower, substructure, foundation	None	None	Static response
	1.3	Tower, substructure, foundation	Fx = 1,500 kN at yaw bearing	None	Static response
Eigen-analysis	2.1	Tower, substructure (clamp at seabed)	None	None	Frequencies, damping, and mode shapes
	2.2	Tower, substructure (clamp at seabed)	None	Still water	Frequencies, damping, and mode shapes
	2.3	Tower, substructure, foundation	None	Still water	Frequencies, damping, and mode shapes
Wind-Only	3.1	Tower, substructure, foundation	Prescribed load time series at yaw bearing V_{hub} = 9.06 m/s	None	Time series (t = 3,600 s)
	3.2	Tower, substructure, foundation	Prescribed load time series at yaw bearing V_{hub} = 20.90 m/s	None	Time series (t = 3,600 s)
Wave-Only	4.1	Tower, substructure, foundation	None	Regular waves: H = 5.50 m, T = 9.0 s	Time series (t = 90 s)
	4.2	Tower, substructure, foundation	None	Irregular waves: Pierson-Moskowitz wave spectrum H_s = 1.25 m, T_p = 5.5 s	Time series (t = 3,600 s)
	4.3	Tower, substructure, foundation	None	Irregular waves: JONSWAP wave spectrum H_s = 7.60 m, T_p = 8.6 s, γ = 5.00	Time series (t = 3,600 s)
Wind + Waves	5.1	Tower, substructure, foundation	Prescribed load time series at yaw bearing V_{hub} = 9.06 m/s	Irregular waves: Pierson-Moskowitz wave spectrum H_s = 1.25 m, T_p = 5.5 s	Time series (t = 3,600 s)
	5.2	Tower, substructure, foundation	Prescribed load time series at yaw bearing V_{hub} = 20.90 m/s	Irregular waves: JONSWAP wave spectrum H_s = 3.75 m, T_p = 7.5 s, γ = 1.37	Time series (t = 3,600 s)

H: regular wave height
H_s: significant wave height
T: regular wave period
T_p: peak-spectral wave period
γ: peak-enhancement factor
V_{hub}: average hub-height wind speed
t: time

5 Outputs

The results for each load case follow the following naming convention to ensure ease in processing the results, e.g., *NAME_LC31.txt*. Each participant chose up to four letters to represent their institution (*NAME*). For those participants using different modeling approaches, the institution name was followed by one number (for example: *NAME1* and *NAME2*). Then, each load case was identified by its two numbers, 31 for LC 3.1, 32 for LC 3.2, etc. The first row of every output file is a header line. The columns are delimited by tab-separated or space-separated values.

For LC 1.X (static analysis), after the initial header line, the second row summarizes the results for LC 1.1, the third line for LC 1.2, etc. Each column provides the static equilibrium value of the loads and offsets described in Table 9. The name of this file is: *NAME_LC1.txt*. The first column "load case number" represents which subcase the participant is focused on, e.g., 1 for LC 1.1, 2 for LC 1.2, and 3 for LC 1.3. It should be noted that all acceleration outputs should be zero for LC 1.X. For fields that are not used in a given simulation, the value should be set to zero.

For the time series cases (LC 3–5), results are summarized in individual files for each load case. So, LC 3.1 and 3.2, for example, are in separate files, named: *NAME_LC31.txt* and *NAME_LC32.txt*. The rows of the time series output files are associated with time steps (remember that the first row is a header line), and the columns as shown in Table 9. The results time step is defined as $\Delta t = 0.05$ s.

All the outputs in Table 9 are expressed in the global coordinate system (Figure 4) except the loads at yaw bearing, tower base, and seabed, which are expressed in a local coordinate system that it is reoriented according to the actual deflection of the structure along the simulation.

Table 9. Output Format for LC 1.X, LC 3.X, LC 4.X, and LC 5.X

Column	Description	Units
1	Simulation time or load case number for LC 1.X	s or -
2	Yaw bearing x displacement	m
3	Yaw bearing y displacement	m
4	Yaw bearing z rotation	deg
5	Yaw bearing x acceleration	m/s^2
6	Yaw bearing y acceleration	m/s^2
7	Yaw bearing fore/aft shear force	N
8	Yaw bearing side/side shear force	N
9	Yaw bearing vertical force	N
10	Yaw bearing fore/aft bending moment	Nm
11	Yaw bearing side/side bending moment	Nm
12	Yaw bearing torque	Nm
13	Tower base x displacement	m
14	Tower base y displacement	m

Column	Description	Units
15	Tower base z rotation	deg
16	Tower base x acceleration	m/s^2
17	Tower base y acceleration	m/s^2
18	Tower base fore/aft shear force	N
19	Tower base side/side shear force	N
20	Tower base vertical force	N
21	Tower base fore/aft bending moment	Nm
22	Tower base side/side bending moment	Nm
23	Tower base torque	Nm
24	Monopile x displacement at seabed	m
25	Monopile y displacement at seabed	m
26	Monopile x rotation at seabed	deg
27	Monopile y rotation at seabed	deg
28	Monopile z rotation at seabed	deg
29	Monopile fore/aft shear force at seabed	N
30	Monopile side/side shear force at seabed	N
31	Monopile vertical force at seabed	N
32	Monopile fore/aft bending moment at seabed	Nm
33	Monopile side/side bending moment at seabed	Nm
34	Monopile torque at seabed	Nm
35	Wave elevation	m

For LC 2.X, the results are presented according to Table 10 and Table 11. Table 10 provides the format to output the eigenfrequencies and damping. After the first row (header line), the second row will summarize results for LC 2.1, and then the third row for LC 2.2, etc. The name of this file should be *NAME_LC2.txt*. Table 11 provides the format to output the mode shapes. After the first row (header line), the next rows describe the mode shape from the seabed to the yaw bearing. For each mode, only the deflection in the principal direction will be reported, e.g., for the fore/aft bending modes, only the displacements along the x direction in the global coordinate system (Figure 4) must be provided. Moreover, the mode shape results are normalized in terms of amplitude. NREL normalized the mode shapes received from the different participants to ensure that the results can be compared consistently. For the different eigen-analyses (LC 2.1, LC 2.2, and LC 2.3), the mode shapes are summarized in individual files, e.g., *NAME_LC21_mode_shapes.txt*, *NAME_LC22_mode_shapes.txt*, etc. Each participant could further discretize the system accounting for additional nodes to perform the proposed analysis, but the nodes used to output the mode shapes had to be aligned with the ones provided in Table 1. For the frequency range up to 2 Hz, it is expected to have the first order bending mode, the second order bending mode, and the first torsional mode.

Table 10. Output Format for LC 2.X: Eigenfrequencies and Damping

Column	Description	Units
1	Load case number	-
2	First fore/aft bending mode	Hz
3	First fore/aft bending mode damping	% of critical damping
4	First side/side bending mode	Hz
5	First side/side bending mode damping	% of critical damping
6	Second fore/aft bending mode	Hz
7	Second fore/aft bending mode damping	% of critical damping
8	Second side/side bending mode	Hz
9	Second side/side bending mode damping	% of critical damping
10	First torsional mode	Hz
11	First torsional bending mode damping	% of critical damping

Table 11. Output Format for LC 2.X: Mode Shapes

Column	Description	Units
1	Node height	m
2	First fore/aft bending mode: Displacement along x axis	m
3	First side/side bending mode: Displacement along y axis	m
4	Second fore/aft bending mode: Displacement along x axis	m
5	Second side/side bending mode: Displacement along y axis	m
6	First torsional mode: Rotation along z axis	rad

References

Anaya-Lara, O., J.O. Tande, K. Uhlen, and K. Merz. 2020. Appendix in *Offshore Wind Energy Technology* (eds O. Anaya-Lara, J.O. Tande, K. Uhlen, and K. Merz). doi:10.1002/9781119097808.app.

Bachynski, E.E., A. Page, and G. Katsikogiannis. 2019. "Dynamic Response of a Large-Diameter Monopile Considering 35-Hour Storm Conditions." In ASME Digital Collection, International Conference on Offshore Mechanics and Arctic Engineering. https://doi.org/10.1115/OMAE2019-95170.

Bortolotti, P., H.C. Tarrés, K. Dykes, L. Merz, D. Sethuraman, D. Verelst, and F. Zahle. 2019. *IEA Wind TCP Task 37: Systems Engineering in Wind Energy - WP2. 1 Reference Wind Turbines.* Golden, CO: National Renewable Energy Laboratory. https://www.nrel.gov/docs/fy19osti/73492.pdf..

Damiani, R., J. Jonkman, and G. Hayman. 2015. *SubDyn User's Guide and Theory Manual.* NREL/TP-5000-63062. Golden, CO: National Renewable Energy Laboratory. https://www.nrel.gov/docs/fy15osti/63062.pdf.

Germanischer, Lloyd. 2010. *Guideline for the Certification of Wind Turbines*. Hamburg: Germanischer Lloyd Industrial Services GmbH. https://www.dnvgl.com/publications/certification-of-wind-turbines-98201.

IEC. 2009. *Wind Turbines – Part 3: Design Requirements for Offshore Wind Turbines.* IEC 61400-3. Geneva: International Electrotechnical Commission.

Katsikogiannis, G., E.E. Bachynski, and A.M. Page. 2019. "Fatigue sensitivity to foundation modelling in different operational states for the DTU 10MW monopile-based offshore wind turbine." J. Phys.: Conf. Ser. 1356 012019. https://iopscience.iop.org/article/10.1088/1742-6596/1356/1/012019

Løken, I.B. 2017. "Dynamic Response and Fatigue of Offshore Wind Turbines." Master of Science Thesis, Norwegian University of Science and Technology.

NGI. 2018. "REDWIN: Reducing cost of offshore wind by integrated structural and geotechnical design." DOC.NO. 201500014-11-R. 3D Foundation Model Library, Norwegian Geotechnical Institute. https://www.ngi.no/eng/Projects/REDWIN-reduce-wind-energy-cost/#Reports-and-publications

Page, A.M., G. Grimstad, G.R. Eiksund, and H.P. Jostad. 2018. "A macro-element pile foundation model for integrated analyses of monopile-based offshore wind turbines." *Ocean Engineering* 167. https://www.sciencedirect.com/science/article/pii/S0029801818315142.

Sivasithamparam, N., B. Misund, A. Page, and A. Løkke. 2020. Doc. 20190610-01-TN "Implementation of REDWIN models in OC6."

Velarde, J. and E.E. Bachynski. 2017. “Design and fatigue analysis of monopile foundations to support the DTU 10 MW offshore wind turbine.” *Energy Procedia* 137. https://www.sciencedirect.com/science/article/pii/S1876610217352906.

Appendix A. Load-Displacement Curves at Seabed

Table A-1 and Table A-2 provide the numerical values for the load-displacement curves at the seabed used for REDWIN model 2. This data is represented graphically in Figure 6 and Figure 7.

Table A-1. Horizontal Displacement and Rotation at Seabed for a Given Overturning Moment

Overturning Moment [Nm]	Horizontal Displacement [m]	Rotation [rad]
0.000000E+00	0.000000E+00	0.000000E+00
1.039356E+07	2.085540E-04	2.509320E-05
1.922284E+07	4.227170E-04	4.859630E-05
2.746240E+07	6.383650E-04	7.140280E-05
3.506780E+07	8.557040E-04	9.342370E-05
4.218780E+07	1.074400E-03	1.148120E-04
4.899800E+07	1.293970E-03	1.357760E-04
5.561000E+07	1.514100E-03	1.564600E-04
6.207540E+07	1.734640E-03	1.769330E-04
6.841120E+07	1.955520E-03	1.972190E-04
7.462260E+07	2.176730E-03	2.173250E-04
8.071460E+07	2.398270E-03	2.372570E-04
8.669460E+07	2.620120E-03	2.570230E-04
9.257280E+07	2.842250E-03	2.766380E-04
9.835900E+07	3.064640E-03	2.961130E-04
1.040622E+08	3.287260E-03	3.154630E-04
1.096898E+08	3.510080E-03	3.346960E-04
1.152472E+08	3.733080E-03	3.538230E-04
1.207392E+08	3.956250E-03	3.728460E-04
1.261702E+08	4.179590E-03	3.917740E-04
1.315460E+08	4.403080E-03	4.106120E-04
1.368692E+08	4.626720E-03	4.293650E-04
1.421424E+08	4.850490E-03	4.480350E-04
1.473706E+08	5.074400E-03	4.666290E-04
1.525566E+08	5.298430E-03	4.851510E-04
1.577030E+08	5.522570E-03	5.036050E-04
1.628122E+08	5.746830E-03	5.219940E-04
1.678852E+08	5.971190E-03	5.403200E-04
1.729224E+08	6.195650E-03	5.585850E-04
1.779256E+08	6.420210E-03	5.767900E-04
1.828962E+08	6.644870E-03	5.949380E-04
1.878344E+08	6.869610E-03	6.130300E-04
1.927408E+08	7.094440E-03	6.310680E-04
1.976160E+08	7.319360E-03	6.490520E-04
2.024600E+08	7.544360E-03	6.669840E-04
2.072740E+08	7.769430E-03	6.848640E-04
2.120580E+08	7.994590E-03	7.026940E-04
2.168140E+08	8.219820E-03	7.204760E-04
2.215420E+08	8.445120E-03	7.382100E-04
2.262440E+08	8.670500E-03	7.558980E-04
2.309180E+08	8.895950E-03	7.735410E-04
2.355660E+08	9.121460E-03	7.911410E-04
2.401900E+08	9.347030E-03	8.086970E-04
2.447900E+08	9.572670E-03	8.262110E-04
2.493660E+08	9.798370E-03	8.436850E-04

Overturning Moment [Nm]	Horizontal Displacement [m]	Rotation [rad]
2.539180E+08	1.002410E-02	8.611180E-04
2.584500E+08	1.024990E-02	8.785130E-04
2.629600E+08	1.047580E-02	8.958700E-04
2.674480E+08	1.070170E-02	9.131910E-04
2.719180E+08	1.092770E-02	9.304750E-04
2.719180E+08	1.092770E-02	9.304750E-04
2.807980E+08	1.137980E-02	9.649380E-04
2.896000E+08	1.183220E-02	9.992630E-04
2.983300E+08	1.228470E-02	1.033450E-03
3.069880E+08	1.273740E-02	1.067520E-03
3.155820E+08	1.319020E-02	1.101460E-03
3.241100E+08	1.364330E-02	1.135280E-03
3.283500E+08	1.386990E-02	1.152150E-03
3.367860E+08	1.432310E-02	1.185800E-03
3.451600E+08	1.477660E-02	1.219350E-03
3.534780E+08	1.523020E-02	1.252780E-03
3.617380E+08	1.568390E-02	1.286110E-03
3.699460E+08	1.613780E-02	1.319340E-03
3.781000E+08	1.659180E-02	1.352460E-03
3.862040E+08	1.704600E-02	1.385500E-03
3.942560E+08	1.750020E-02	1.418440E-03
4.022600E+08	1.795460E-02	1.451280E-03
4.102180E+08	1.840920E-02	1.484040E-03
4.181280E+08	1.886380E-02	1.516710E-03
4.220680E+08	1.909120E-02	1.533020E-03
4.299120E+08	1.954600E-02	1.565560E-03
4.377140E+08	2.000090E-02	1.598020E-03
4.454720E+08	2.045590E-02	1.630390E-03
4.531880E+08	2.091110E-02	1.662690E-03
4.608640E+08	2.136630E-02	1.694910E-03
4.685020E+08	2.182170E-02	1.727050E-03
4.761000E+08	2.227710E-02	1.759120E-03
4.836600E+08	2.273270E-02	1.791110E-03
4.911820E+08	2.318830E-02	1.823030E-03
4.986680E+08	2.364400E-02	1.854880E-03
5.061180E+08	2.409990E-02	1.886650E-03
5.135320E+08	2.455580E-02	1.918360E-03
5.172260E+08	2.478380E-02	1.934190E-03
5.245900E+08	2.523980E-02	1.965790E-03
5.319180E+08	2.569590E-02	1.997330E-03
5.392140E+08	2.615220E-02	2.028800E-03
5.464780E+08	2.660850E-02	2.060210E-03
5.537100E+08	2.706480E-02	2.091550E-03
5.609080E+08	2.752130E-02	2.122830E-03
5.680760E+08	2.797780E-02	2.154050E-03
5.752160E+08	2.843450E-02	2.185210E-03
5.823260E+08	2.889120E-02	2.216310E-03
5.894060E+08	2.934790E-02	2.247340E-03
5.964560E+08	2.980480E-02	2.278320E-03
5.999700E+08	3.003320E-02	2.293790E-03
6.069760E+08	3.049020E-02	2.324680E-03
6.139560E+08	3.094720E-02	2.355520E-03

Overturning Moment [Nm]	Horizontal Displacement [m]	Rotation [rad]
6.209080E+08	3.140430E-02	2.386300E-03
6.278320E+08	3.186140E-02	2.417030E-03
6.347280E+08	3.231870E-02	2.447690E-03
6.415980E+08	3.277600E-02	2.478310E-03
6.484420E+08	3.323330E-02	2.508870E-03
6.552600E+08	3.369070E-02	2.539380E-03
6.620500E+08	3.414820E-02	2.569830E-03
6.688140E+08	3.460580E-02	2.600240E-03
6.755540E+08	3.506340E-02	2.630590E-03
6.789140E+08	3.529220E-02	2.645740E-03
6.856160E+08	3.574990E-02	2.676020E-03
6.922940E+08	3.620770E-02	2.706240E-03
6.989480E+08	3.666550E-02	2.736420E-03
7.055760E+08	3.712340E-02	2.766540E-03
7.121800E+08	3.758130E-02	2.796620E-03
7.187620E+08	3.803940E-02	2.826640E-03
7.253200E+08	3.849740E-02	2.856620E-03
7.318520E+08	3.895550E-02	2.886550E-03
7.383620E+08	3.941370E-02	2.916430E-03
7.448520E+08	3.987190E-02	2.946270E-03
7.513180E+08	4.033020E-02	2.976060E-03
7.577620E+08	4.078860E-02	3.005800E-03
7.609760E+08	4.101770E-02	3.020660E-03
7.673860E+08	4.147620E-02	3.050330E-03
7.737740E+08	4.193460E-02	3.079960E-03
7.801420E+08	4.239320E-02	3.109550E-03
7.864880E+08	4.285170E-02	3.139090E-03
7.928140E+08	4.331030E-02	3.168590E-03
7.991160E+08	4.376900E-02	3.198040E-03
8.053960E+08	4.422780E-02	3.227450E-03
8.116560E+08	4.468650E-02	3.256810E-03
8.178980E+08	4.514540E-02	3.286140E-03
8.241200E+08	4.560420E-02	3.315420E-03
8.303200E+08	4.606310E-02	3.344660E-03
8.334120E+08	4.629260E-02	3.359260E-03
8.395800E+08	4.675160E-02	3.388430E-03
8.457300E+08	4.721070E-02	3.417570E-03
8.518600E+08	4.766980E-02	3.446660E-03
8.579700E+08	4.812890E-02	3.475710E-03
8.640620E+08	4.858810E-02	3.504720E-03
8.701340E+08	4.904730E-02	3.533690E-03
8.761900E+08	4.950660E-02	3.562620E-03
8.822260E+08	4.996590E-02	3.591520E-03
8.882440E+08	5.042530E-02	3.620370E-03
8.942440E+08	5.088470E-02	3.649180E-03
9.002240E+08	5.134420E-02	3.677950E-03
9.061880E+08	5.180370E-02	3.706690E-03
9.091620E+08	5.203350E-02	3.721040E-03
9.150980E+08	5.249300E-02	3.749720E-03
9.210140E+08	5.295260E-02	3.778370E-03
9.269120E+08	5.341230E-02	3.806970E-03
9.327900E+08	5.387200E-02	3.835530E-03

Overturning Moment [Nm]	Horizontal Displacement [m]	Rotation [rad]
9.386500E+08	5.433170E-02	3.864050E-03
9.444920E+08	5.479150E-02	3.892540E-03
9.503180E+08	5.525130E-02	3.920990E-03
9.561220E+08	5.571120E-02	3.949400E-03
9.619080E+08	5.617110E-02	3.977770E-03
9.676760E+08	5.663110E-02	4.006100E-03
9.734280E+08	5.709110E-02	4.034400E-03
9.762980E+08	5.732110E-02	4.048540E-03
9.820240E+08	5.778110E-02	4.076780E-03
9.877340E+08	5.824120E-02	4.104990E-03
9.934260E+08	5.870140E-02	4.133160E-03
9.990980E+08	5.916150E-02	4.161290E-03
1.004754E+09	5.962180E-02	4.189390E-03
1.010392E+09	6.008200E-02	4.217450E-03
1.016012E+09	6.054230E-02	4.245470E-03
1.021614E+09	6.100270E-02	4.273460E-03
1.027202E+09	6.146300E-02	4.301410E-03
1.032772E+09	6.192350E-02	4.329320E-03
1.038326E+09	6.238390E-02	4.357200E-03
1.041098E+09	6.261420E-02	4.371130E-03
1.046626E+09	6.307470E-02	4.398960E-03
1.052140E+09	6.353520E-02	4.426750E-03
1.057638E+09	6.399580E-02	4.454510E-03
1.063120E+09	6.445650E-02	4.482230E-03
1.068586E+09	6.491710E-02	4.509920E-03
1.074038E+09	6.537780E-02	4.537580E-03
1.079474E+09	6.583860E-02	4.565200E-03
1.084898E+09	6.629930E-02	4.592800E-03
1.090306E+09	6.676020E-02	4.620360E-03
1.095696E+09	6.722100E-02	4.647890E-03
1.101074E+09	6.768190E-02	4.675380E-03
1.106434E+09	6.814280E-02	4.702840E-03
1.109110E+09	6.837330E-02	4.716560E-03
1.114446E+09	6.883430E-02	4.743970E-03
1.119768E+09	6.929530E-02	4.771350E-03
1.125076E+09	6.975630E-02	4.798690E-03
1.130372E+09	7.021740E-02	4.826010E-03
1.135652E+09	7.067850E-02	4.853290E-03
1.140916E+09	7.113970E-02	4.880540E-03
1.146168E+09	7.160090E-02	4.907770E-03
1.151406E+09	7.206210E-02	4.934960E-03
1.156632E+09	7.252340E-02	4.962120E-03
1.161844E+09	7.298460E-02	4.989250E-03
1.167040E+09	7.344600E-02	5.016350E-03
1.169632E+09	7.367660E-02	5.029890E-03
1.174806E+09	7.413800E-02	5.056940E-03
1.179966E+09	7.459940E-02	5.083960E-03
1.185114E+09	7.506080E-02	5.110950E-03
1.190248E+09	7.552230E-02	5.137920E-03
1.195366E+09	7.598380E-02	5.164850E-03
1.200000E+09	7.640300E-02	5.189280E-03

Table A-2. Horizontal Displacement and Rotation at Seabed for a Given Horizontal Force

Horizontal Force [N]	Horizontal Displacement [m]	Rotation [rad]
0.000000E+00	0.000000E+00	0.000000E+00
1.758156E+05	5.434320E-05	3.191960E-06
3.414300E+05	1.088750E-04	6.407050E-06
4.923000E+05	1.637020E-04	9.623900E-06
6.337100E+05	2.187290E-04	1.283210E-05
7.681160E+05	2.738740E-04	1.602500E-05
8.950960E+05	3.291770E-04	1.919740E-05
1.018308E+06	3.844950E-04	2.235450E-05
1.136352E+06	4.398400E-04	2.548820E-05
1.247398E+06	4.953550E-04	2.859450E-05
1.357410E+06	5.508720E-04	3.169600E-05
1.465010E+06	6.064020E-04	3.478450E-05
1.569666E+06	6.619520E-04	3.785620E-05
1.671532E+06	7.175210E-04	4.091140E-05
1.771022E+06	7.731060E-04	4.395200E-05
1.868520E+06	8.287040E-04	4.698060E-05
1.964258E+06	8.843140E-04	4.999830E-05
2.058360E+06	9.399350E-04	5.300560E-05
2.150880E+06	9.955670E-04	5.600270E-05
2.241920E+06	1.051210E-03	5.898990E-05
2.331620E+06	1.106860E-03	6.196740E-05
2.420000E+06	1.162520E-03	6.493550E-05
2.507180E+06	1.218200E-03	6.789450E-05
2.593220E+06	1.273880E-03	7.084470E-05
2.678200E+06	1.329570E-03	7.378680E-05
2.762120E+06	1.385280E-03	7.672060E-05
2.845060E+06	1.440990E-03	7.964640E-05
2.927060E+06	1.496710E-03	8.256440E-05
3.008160E+06	1.552430E-03	8.547510E-05
3.088440E+06	1.608170E-03	8.837840E-05
3.167900E+06	1.663910E-03	9.127470E-05
3.246580E+06	1.719670E-03	9.416410E-05
3.324540E+06	1.775430E-03	9.704710E-05
3.401780E+06	1.831190E-03	9.992360E-05
3.478340E+06	1.886960E-03	1.027940E-04
3.554240E+06	1.942740E-03	1.056580E-04
3.629520E+06	1.998530E-03	1.085160E-04
3.704160E+06	2.054320E-03	1.113680E-04
3.778200E+06	2.110120E-03	1.142150E-04
3.851680E+06	2.165920E-03	1.170560E-04
3.924580E+06	2.221730E-03	1.198920E-04
3.996940E+06	2.277550E-03	1.227230E-04
4.068780E+06	2.333370E-03	1.255480E-04
4.140120E+06	2.389190E-03	1.283680E-04
4.210960E+06	2.445020E-03	1.311840E-04
4.281320E+06	2.500860E-03	1.339950E-04
4.351200E+06	2.556700E-03	1.368010E-04
4.420620E+06	2.612540E-03	1.396030E-04
4.489620E+06	2.668390E-03	1.424000E-04
4.558200E+06	2.724240E-03	1.451930E-04

Horizontal Force [N]	Horizontal Displacement [m]	Rotation [rad]
4.558200E+06	2.724240E-03	1.451930E-04
4.694080E+06	2.835960E-03	1.507660E-04
4.828340E+06	2.947690E-03	1.563220E-04
4.961140E+06	3.059440E-03	1.618610E-04
5.092540E+06	3.171200E-03	1.673840E-04
5.222560E+06	3.282980E-03	1.728920E-04
5.351300E+06	3.394780E-03	1.783840E-04
5.478800E+06	3.506580E-03	1.838630E-04
5.605100E+06	3.618410E-03	1.893270E-04
5.730240E+06	3.730240E-03	1.947770E-04
5.792400E+06	3.786160E-03	1.974980E-04
5.915900E+06	3.898010E-03	2.029290E-04
6.038320E+06	4.009880E-03	2.083480E-04
6.159700E+06	4.121750E-03	2.137540E-04
6.280080E+06	4.233630E-03	2.191480E-04
6.399500E+06	4.345530E-03	2.245320E-04
6.518000E+06	4.457430E-03	2.299040E-04
6.635560E+06	4.569340E-03	2.352650E-04
6.752260E+06	4.681260E-03	2.406150E-04
6.868100E+06	4.793190E-03	2.459540E-04
6.983140E+06	4.905130E-03	2.512830E-04
7.097340E+06	5.017080E-03	2.566020E-04
7.210780E+06	5.129030E-03	2.619100E-04
7.323460E+06	5.241000E-03	2.672080E-04
7.435380E+06	5.352970E-03	2.724960E-04
7.546580E+06	5.464950E-03	2.777750E-04
7.657080E+06	5.576930E-03	2.830450E-04
7.766880E+06	5.688920E-03	2.883050E-04
7.821520E+06	5.744920E-03	2.909320E-04
7.930320E+06	5.856930E-03	2.961790E-04
8.038460E+06	5.968940E-03	3.014180E-04
8.145960E+06	6.080960E-03	3.066480E-04
8.252840E+06	6.192980E-03	3.118690E-04
8.359100E+06	6.305010E-03	3.170830E-04
8.464760E+06	6.417050E-03	3.222880E-04
8.569820E+06	6.529100E-03	3.274850E-04
8.674300E+06	6.641150E-03	3.326750E-04
8.778220E+06	6.753210E-03	3.378570E-04
8.881580E+06	6.865270E-03	3.430310E-04
8.984420E+06	6.977340E-03	3.481980E-04
9.086720E+06	7.089420E-03	3.533580E-04
9.188500E+06	7.201500E-03	3.585100E-04
9.289760E+06	7.313590E-03	3.636550E-04
9.390500E+06	7.425690E-03	3.687930E-04
9.490720E+06	7.537790E-03	3.739240E-04
9.590460E+06	7.649900E-03	3.790490E-04
9.689680E+06	7.762010E-03	3.841670E-04
9.739100E+06	7.818070E-03	3.867230E-04
9.837600E+06	7.930190E-03	3.918310E-04
9.935620E+06	8.042320E-03	3.969320E-04
1.003318E+07	8.154450E-03	4.020270E-04
1.013028E+07	8.266590E-03	4.071160E-04

Horizontal Force [N]	Horizontal Displacement [m]	Rotation [rad]
1.022692E+07	8.378730E-03	4.121990E-04
1.032314E+07	8.490880E-03	4.172750E-04
1.041892E+07	8.603040E-03	4.223450E-04
1.051430E+07	8.715200E-03	4.274100E-04
1.060924E+07	8.827360E-03	4.324680E-04
1.070380E+07	8.939530E-03	4.375210E-04
1.079796E+07	9.051700E-03	4.425670E-04
1.089170E+07	9.163880E-03	4.476080E-04
1.098506E+07	9.276060E-03	4.526430E-04
1.107804E+07	9.388250E-03	4.576730E-04
1.117064E+07	9.500440E-03	4.626970E-04
1.126286E+07	9.612630E-03	4.677160E-04
1.135472E+07	9.724830E-03	4.727290E-04
1.144622E+07	9.837030E-03	4.777360E-04
1.149184E+07	9.893140E-03	4.802380E-04
1.158278E+07	1.000530E-02	4.852380E-04
1.167340E+07	1.011760E-02	4.902320E-04
1.176366E+07	1.022980E-02	4.952220E-04
1.185358E+07	1.034200E-02	5.002060E-04
1.194318E+07	1.045420E-02	5.051860E-04
1.203244E+07	1.056650E-02	5.101610E-04
1.212136E+07	1.067870E-02	5.151310E-04
1.220998E+07	1.079090E-02	5.200960E-04
1.229824E+07	1.090320E-02	5.250560E-04
1.238618E+07	1.101540E-02	5.300120E-04
1.247386E+07	1.112770E-02	5.349620E-04
1.256122E+07	1.123990E-02	5.399080E-04
1.264828E+07	1.135220E-02	5.448500E-04
1.273504E+07	1.146440E-02	5.497860E-04
1.282148E+07	1.157670E-02	5.547190E-04
1.290762E+07	1.168900E-02	5.596460E-04
1.299350E+07	1.180120E-02	5.645690E-04
1.303632E+07	1.185740E-02	5.670290E-04
1.312176E+07	1.196960E-02	5.719460E-04
1.320692E+07	1.208190E-02	5.768580E-04
1.329180E+07	1.219420E-02	5.817660E-04
1.337642E+07	1.230650E-02	5.866690E-04
1.346076E+07	1.241880E-02	5.915690E-04
1.354482E+07	1.253110E-02	5.964640E-04
1.362862E+07	1.264340E-02	6.013540E-04
1.371216E+07	1.275560E-02	6.062410E-04
1.379544E+07	1.286790E-02	6.111230E-04
1.387848E+07	1.298030E-02	6.160010E-04
1.396124E+07	1.309260E-02	6.208760E-04
1.404376E+07	1.320490E-02	6.257460E-04
1.412604E+07	1.331720E-02	6.306120E-04
1.420806E+07	1.342950E-02	6.354740E-04
1.428984E+07	1.354180E-02	6.403330E-04
1.437138E+07	1.365410E-02	6.451870E-04
1.445268E+07	1.376640E-02	6.500380E-04
1.453374E+07	1.387880E-02	6.548850E-04
1.457416E+07	1.393490E-02	6.573070E-04

Horizontal Force [N]	Horizontal Displacement [m]	Rotation [rad]
1.465488E+07	1.404730E-02	6.621480E-04
1.473534E+07	1.415960E-02	6.669850E-04
1.481558E+07	1.427190E-02	6.718190E-04
1.489558E+07	1.438430E-02	6.766490E-04
1.497538E+07	1.449660E-02	6.814750E-04
1.505494E+07	1.460900E-02	6.862980E-04
1.513430E+07	1.472130E-02	6.911170E-04
1.521344E+07	1.483370E-02	6.959320E-04
1.529234E+07	1.494600E-02	7.007440E-04
1.537104E+07	1.505840E-02	7.055520E-04
1.544952E+07	1.517070E-02	7.103570E-04
1.552780E+07	1.528310E-02	7.151590E-04
1.560584E+07	1.539540E-02	7.199570E-04
1.568370E+07	1.550780E-02	7.247510E-04
1.576136E+07	1.562020E-02	7.295420E-04
1.583880E+07	1.573250E-02	7.343300E-04
1.591602E+07	1.584490E-02	7.391140E-04
1.599306E+07	1.595730E-02	7.438950E-04
1.603152E+07	1.601350E-02	7.462840E-04
1.610826E+07	1.612580E-02	7.510600E-04
1.618482E+07	1.623820E-02	7.558330E-04
1.626118E+07	1.635060E-02	7.606020E-04
1.633736E+07	1.646300E-02	7.653680E-04
1.641334E+07	1.657540E-02	7.701310E-04
1.648912E+07	1.668780E-02	7.748900E-04
1.656474E+07	1.680020E-02	7.796470E-04
1.664016E+07	1.691250E-02	7.844000E-04
1.671538E+07	1.702490E-02	7.891500E-04
1.679042E+07	1.713730E-02	7.938980E-04
1.686528E+07	1.724970E-02	7.986420E-04
1.693996E+07	1.736210E-02	8.033830E-04
1.701446E+07	1.747450E-02	8.081210E-04
1.708880E+07	1.758700E-02	8.128560E-04
1.716294E+07	1.769940E-02	8.175880E-04
1.723690E+07	1.781180E-02	8.223170E-04
1.731068E+07	1.792420E-02	8.270430E-04
1.734750E+07	1.798040E-02	8.294050E-04
1.742104E+07	1.809280E-02	8.341260E-04
1.749440E+07	1.820520E-02	8.388450E-04
1.756758E+07	1.831760E-02	8.435610E-04
1.764062E+07	1.843010E-02	8.482740E-04
1.771344E+07	1.854250E-02	8.529840E-04
1.778614E+07	1.865490E-02	8.576910E-04
1.785866E+07	1.876730E-02	8.623950E-04
1.793100E+07	1.887980E-02	8.670960E-04
1.800000E+07	1.898730E-02	8.715880E-04

Appendix B. Nonlinear *p-y* Curves Along the Monopile

Table B-1 provides the numerical values for the 61 nonlinear *p-y* curves at different depths along the monopile. Part of this data is represented graphically in Figure 11. The depth indicated in Table B-1 follows the same convention as the one shown in Table 1.

Table B-1. *p-y* Curves Along the Monopile

Spring #01	
Depth: 0.00 m	
p [N/m]	y [m]
0.00	0.000000
259.08	0.001846
366.20	0.003032
517.38	0.005129
730.22	0.008935
892.56	0.012521
1028.59	0.015992
1147.72	0.019390
1607.21	0.035788
2229.23	0.067292
2678.72	0.098047
3035.85	0.128399
3332.47	0.158489
4320.08	0.306783
4884.00	0.453235
5236.73	0.598768
5464.52	0.743759
5611.95	0.888400
5705.04	1.032805
5760.11	1.177044
5796.00	1.465200
5796.00	144.025200

Spring #02	
Depth: -0.75 m	
p [N/m]	y [m]
0.00	0.000000
17750.48	0.000989
25090.43	0.001624
35447.81	0.002748
50030.91	0.004787
61153.28	0.006708
70473.62	0.008567
78635.88	0.010388
110117.70	0.019172
152735.10	0.036049
183532.00	0.052525
208000.00	0.068785
228322.90	0.084905
295989.20	0.164348
334625.80	0.242804
358793.10	0.320769
374400.00	0.398442
384501.30	0.475928
390878.90	0.553288
394652.30	0.630559
397111.20	0.784929
397111.20	77.156360

Spring #03	
Depth: -1.50 m	
p [N/m]	y [m]
0.00	0.000000
37187.46	0.000989
52564.75	0.001624
74263.59	0.002748
104815.40	0.004787
128116.90	0.006708
147643.10	0.008567
164743.10	0.010388
230697.80	0.019172
319981.80	0.036049
384501.80	0.052525
435762.50	0.068785
478339.20	0.084905
620101.00	0.164348
701045.00	0.242804
751675.90	0.320769
784372.60	0.398442
805534.80	0.475928
818896.00	0.553288
826801.30	0.630559
831952.70	0.784929
831952.70	77.156360

Spring #04	
Depth: -2.25 m	
p [N/m]	y [m]
0.00	0.000000
58008.15	0.000989
81994.93	0.001624
115842.60	0.002748
163499.90	0.004787
199847.50	0.006708
230306.20	0.008567
256980.20	0.010388
359861.90	0.019172
499134.70	0.036049
599778.40	0.052525
679739.20	0.068785
746153.90	0.084905
967285.80	0.164348
1093549.00	0.242804

Spring #05	
Depth: -3.00 m	
p [N/m]	y [m]
0.00	0.000000
79989.11	0.000989
113065.20	0.001624
159738.70	0.002748
225454.70	0.004787
275575.50	0.006708
317575.80	0.008567
354357.50	0.010388
496224.00	0.019172
688271.20	0.036049
827051.80	0.052525
937312.10	0.068785
1028893.00	0.084905
1333818.00	0.164348
1507927.00	0.242804

Spring #06	
Depth: -3.75 m	
p [N/m]	y [m]
0.00	0.000000
102995.30	0.000989
145584.60	0.001624
205682.30	0.002748
290299.30	0.004787
354835.70	0.006708
408916.00	0.008567
456276.70	0.010388
638946.50	0.019172
886229.70	0.036049
1064926.00	0.052525
1206899.00	0.068785
1324820.00	0.084905
1717447.00	0.164348
1941632.00	0.242804

Spring #04	
Depth: -2.25 m	
p [N/m]	y [m]
1172528.00	0.320769
1223531.00	0.398442
1256541.00	0.475928
1277383.00	0.553288
1289714.00	0.630559
1297750.00	0.784929
1297750.00	77.156360

Spring #05	
Depth: -3.00 m	
p [N/m]	y [m]
1616832.00	0.320769
1687162.00	0.398442
1732681.00	0.475928
1761421.00	0.553288
1778425.00	0.630559
1789505.00	0.784929
1789505.00	77.156360

Spring #06	
Depth: -3.75 m	
p [N/m]	y [m]
2081860.00	0.320769
2172418.00	0.398442
2231029.00	0.475928
2268035.00	0.553288
2289930.00	0.630559
2304197.00	0.784929
2304197.00	77.156360

Spring #07	
Depth: -4.50 m	
p [N/m]	y [m]
0.00	0.000000
126932.80	0.000993
179420.40	0.001631
253485.50	0.002759
357768.60	0.004805
437304.10	0.006733
503953.40	0.008600
562321.30	0.010428
787445.90	0.019246
1092201.00	0.036189
1312429.00	0.052728
1487398.00	0.069051
1632726.00	0.085233
2116604.00	0.164984
2392893.00	0.243744
2565712.00	0.322010
2677316.00	0.399984
2749550.00	0.477770
2795156.00	0.555429
2822139.00	0.632999
2839723.00	0.787965
2839723.00	77.454880

Spring #08	
Depth: -5.25 m	
p [N/m]	y [m]
0.00	0.000000
151730.70	0.000994
214472.40	0.001632
303007.10	0.002760
427663.10	0.004808
522736.90	0.006737
602407.00	0.008605
672177.80	0.010434
941283.30	0.019258
1305576.00	0.036210
1568828.00	0.052759
1777980.00	0.069092
1951699.00	0.085284
2530109.00	0.165082
2860374.00	0.243888
3066956.00	0.322201
3200363.00	0.400221
3286708.00	0.478053
3341224.00	0.555758
3373479.00	0.633374
3394498.00	0.788433
3394498.00	77.500810

Spring #09	
Depth: -6.00 m	
p [N/m]	y [m]
0.00	0.000000
177333.00	0.001010
250661.50	0.001659
354135.20	0.002806
499825.10	0.004888
610941.20	0.006849
704054.40	0.008748
785598.00	0.010607
1100111.00	0.019577
1525873.00	0.036811
1833545.00	0.053635
2077988.00	0.070239
2281020.00	0.086699
2957029.00	0.167821
3343021.00	0.247935
3584460.00	0.327547
3740378.00	0.406862
3841293.00	0.485985
3905007.00	0.564980
3942705.00	0.643884
3967270.00	0.801515
3967270.00	78.786740

Spring #10	
Depth: -6.75 m	
p [N/m]	y [m]
0.00	0.000000
203694.00	0.001010
287922.90	0.001659
406778.10	0.002806
574125.10	0.004888
701758.90	0.006849
808713.60	0.008748
902378.80	0.010607
1263645.00	0.019577

Spring #11	
Depth: -7.50 m	
p [N/m]	y [m]
0.00	0.000000
230774.90	0.001010
326202.00	0.001659
460858.90	0.002806
650454.60	0.004888
795057.10	0.006849
916231.30	0.008748
1022349.00	0.010607
1431646.00	0.019577

Spring #12	
Depth: -8.25 m	
p [N/m]	y [m]
0.00	0.000000
258542.80	0.001034
365452.10	0.001698
516311.50	0.002873
728720.20	0.005004
890721.90	0.007013
1026476.00	0.008957
1145363.00	0.010861
1603908.00	0.020045

Spring #10	
Depth: -6.75 m	
p [N/m]	y [m]
1752697.00	0.036811
2106105.00	0.053635
2386885.00	0.070239
2620098.00	0.086699
3396597.00	0.167821
3839967.00	0.247935
4117297.00	0.327547
4296393.00	0.406862
4412309.00	0.485985
4485495.00	0.564980
4528796.00	0.643884
4557013.00	0.801515
4557013.00	78.786740

Spring #11	
Depth: -7.50 m	
p [N/m]	y [m]
1985717.00	0.036811
2386110.00	0.053635
2704219.00	0.070239
2968438.00	0.086699
3848172.00	0.167821
4350488.00	0.247935
4664688.00	0.327547
4867595.00	0.406862
4998922.00	0.485985
5081838.00	0.564980
5130895.00	0.643884
5162864.00	0.801515
5162864.00	78.786740

Spring #12	
Depth: -8.25 m	
p [N/m]	y [m]
2224647.00	0.037691
2673217.00	0.054917
3029603.00	0.071918
3325614.00	0.088771
4311201.00	0.171832
4873958.00	0.253861
5225965.00	0.335375
5453286.00	0.416586
5600414.00	0.497600
5693307.00	0.578483
5748268.00	0.659272
5784083.00	0.820671
5784083.00	80.669730

Spring #13	
Depth: -9.00 m	
p [N/m]	y [m]
0.00	0.000000
286968.80	0.001027
405632.40	0.001686
573078.30	0.002852
808840.70	0.004967
988654.10	0.006961
1139334.00	0.008891
1271292.00	0.010780
1780252.00	0.019897
2469240.00	0.037412
2967129.00	0.054510
3362699.00	0.071385
3691255.00	0.088114
4785204.00	0.170560
5409835.00	0.251982
5800543.00	0.332893
6052858.00	0.413502
6216163.00	0.493917
6319269.00	0.574201
6380272.00	0.654393
6420025.00	0.814597
6420025.00	80.072680

Spring #14	
Depth: -9.75 m	
p [N/m]	y [m]
0.00	0.000000
316027.40	0.001027
446707.10	0.001686
631108.70	0.002852
890744.50	0.004967
1088766.00	0.006961
1254704.00	0.008891
1400024.00	0.010780
1960522.00	0.019897
2719278.00	0.037412
3267583.00	0.054510
3703208.00	0.071385
4065034.00	0.088114
5269758.00	0.170560
5957639.00	0.251982
6387911.00	0.332893
6665775.00	0.413502
6845616.00	0.493917
6959163.00	0.574201
7026343.00	0.654393
7070122.00	0.814597
7070122.00	80.072680

Spring #15	
Depth: -10.50 m	
p [N/m]	y [m]
0.00	0.000000
345696.10	0.001030
488644.00	0.001692
690357.20	0.002862
974367.70	0.004986
1190979.00	0.006987
1372496.00	0.008924
1531459.00	0.010820
2144576.00	0.019971
2974564.00	0.037552
3574344.00	0.054714
4050866.00	0.071651
4446660.00	0.088443
5764483.00	0.171196
6516942.00	0.252921
6987609.00	0.334134
7291558.00	0.415044
7488283.00	0.495759
7612490.00	0.576342
7685977.00	0.656833
7733865.00	0.817634
7733865.00	80.371210

Spring #16	
Depth: -11.25 m	
p [N/m]	y [m]
0.00	0.000000
375954.40	0.001047
531414.20	0.001719

Spring #17	
Depth: -12.00 m	
p [N/m]	y [m]
0.00	0.000000
406783.70	0.001041
574991.70	0.001710

Spring #18	
Depth: -12.75 m	
p [N/m]	y [m]
0.00	0.000000
438167.20	0.001061
619352.50	0.001743

Spring #16	
Depth: -11.25 m	
p [N/m]	y [m]
750783.20	0.002908
1059653.00	0.005066
1295224.00	0.007099
1492628.00	0.009067
1665505.00	0.010993
2332288.00	0.020290
3234923.00	0.038152
3887201.00	0.055589
4405432.00	0.072798
4835870.00	0.089858
6269040.00	0.173935
7087361.00	0.256968
7599224.00	0.339480
7929778.00	0.421685
8143721.00	0.503691
8278800.00	0.585563
8358720.00	0.667342
8410799.00	0.830716
8410799.00	81.657140

Spring #17	
Depth: -12.00 m	
p [N/m]	y [m]
812349.60	0.002893
1146547.00	0.005039
1401436.00	0.007062
1615028.00	0.009019
1802081.00	0.010936
2523542.00	0.020184
3500196.00	0.037952
4205963.00	0.055297
4766690.00	0.072416
5232425.00	0.089386
6783119.00	0.173022
7668545.00	0.255619
8222382.00	0.337698
8580042.00	0.419471
8811530.00	0.501047
8957685.00	0.582489
9044158.00	0.663839
9100509.00	0.826355
9100509.00	81.228500

Spring #18	
Depth: -12.75 m	
p [N/m]	y [m]
875022.60	0.002948
1235004.00	0.005136
1509557.00	0.007197
1739628.00	0.009192
1941112.00	0.011145
2718234.00	0.020570
3770237.00	0.038678
4530454.00	0.056355
5134442.00	0.073801
5636108.00	0.091096
7306438.00	0.176332
8260175.00	0.260509
8856741.00	0.344158
9241995.00	0.427495
9491342.00	0.510632
9648773.00	0.593632
9741918.00	0.676538
9802616.00	0.842163
9802616.00	82.782340

Spring #19	
Depth: -13.50 m	
p [N/m]	y [m]
0.00	0.000000
470089.30	0.001078
664474.60	0.001770
938771.10	0.002994
1324978.00	0.005215
1619534.00	0.007308
1866366.00	0.009335
2082529.00	0.011318
2916267.00	0.020890
4044912.00	0.039279
4860514.00	0.057230
5508504.00	0.074947
6046719.00	0.092511
7838739.00	0.179071
8861959.00	0.264556
9501987.00	0.349504
9915308.00	0.434136
10182820.00	0.518564
10351720.00	0.602854
10451650.00	0.687047
10516770.00	0.855245
10516770.00	84.068280

Spring #20	
Depth: -14.25 m	
p [N/m]	y [m]
0.00	0.000000
502535.60	0.001076
710337.70	0.001767
1003567.00	0.002988
1416430.00	0.005205
1731317.00	0.007294
1995186.00	0.009317
2226269.00	0.011296
3117553.00	0.020850
4324099.00	0.039204
5195995.00	0.057121
5888710.00	0.074804
6464073.00	0.092334
8379782.00	0.178729
9473626.00	0.264050
10157830.00	0.348836
10599680.00	0.433306
10885660.00	0.517572
11066210.00	0.601701
11173040.00	0.685733
11242660.00	0.853610
11242660.00	83.907540

Spring #21	
Depth: -15.00 m	
p [N/m]	y [m]
0.00	0.000000
535492.90	0.001092
756923.10	0.001794
1069383.00	0.003034
1509323.00	0.005285
1844860.00	0.007406
2126034.00	0.009460
2372272.00	0.011470
3322008.00	0.021169
4607682.00	0.039805
5536758.00	0.057996
6274903.00	0.075950
6888000.00	0.093749
8929344.00	0.181468
10094920.00	0.268097
10824000.00	0.354182
11294830.00	0.439947
11599560.00	0.525504
11791960.00	0.610922
11905790.00	0.696242
11979970.00	0.866692
11979970.00	85.193480

Spring #22	
Depth: -15.75 m	
p [N/m]	y [m]
0.00	0.000000
568948.70	0.001092
804213.10	0.001794
1136194.00	0.003034
1603620.00	0.005285
1960121.00	0.007406
2258862.00	0.009460
2520483.00	0.011470
3529556.00	0.021169
4895554.00	0.039805
5882677.00	0.057996
6666938.00	0.075950
7318339.00	0.093749
9487220.00	0.181468
10725620.00	0.268097
11500250.00	0.354182
12000490.00	0.439947
12324260.00	0.525504
12528680.00	0.610922
12649630.00	0.696242
12728440.00	0.866692
12728440.00	85.193480

Spring #23	
Depth: -16.50 m	
p [N/m]	y [m]
0.00	0.000000
602891.50	0.001117
852191.40	0.001834
1203978.00	0.003103
1699290.00	0.005405
2077059.00	0.007574
2393623.00	0.009674
2670852.00	0.011729
3740124.00	0.021648
5187617.00	0.040706
6233629.00	0.059309
7064679.00	0.077670
7754942.00	0.095872
10053220.00	0.185576
11365500.00	0.274167
12186340.00	0.362201
12716420.00	0.449908
13059510.00	0.537403
13276120.00	0.624754
13404290.00	0.712006
13487800.00	0.886315
13487800.00	87.122390

Spring #24	
Depth: -17.25 m	
p [N/m]	y [m]
0.00	0.000000
637310.30	0.001117
900842.60	0.001834
1272712.00	0.003103
1796302.00	0.005405
2195638.00	0.007574
2530274.00	0.009674
2823330.00	0.011729
3953647.00	0.021648
5483776.00	0.040706
6589505.00	0.059309
7467999.00	0.077670
8197668.00	0.095872
10627150.00	0.185576
12014350.00	0.274167
12882050.00	0.362201
13442400.00	0.449908
13805070.00	0.537403
14034050.00	0.624754
14169530.00	0.712006
14257820.00	0.886315
14257820.00	87.122390

Spring #25	
Depth: -18.00 m	
p [N/m]	y [m]
0.00	0.000000
672194.90	0.001117
950152.40	0.001834
1342377.00	0.003103
1894627.00	0.005405
2315821.00	0.007574
2668774.00	0.009674
2977871.00	0.011729
4170059.00	0.021648
5783943.00	0.040706
6950197.00	0.059309
7876777.00	0.077670
8646386.00	0.095872
11208850.00	0.185576
12671980.00	0.274167
13587180.00	0.362201
14178200.00	0.449908
14560720.00	0.537403
14802240.00	0.624754
14945130.00	0.712006
15038250.00	0.886315
15038250.00	87.122390

Spring #26	
Depth: -18.75 m	
p [N/m]	y [m]
0.00	0.000000
707535.80	0.001150
1000107.00	0.001888
1412953.00	0.003194
1994237.00	0.005564
2437576.00	0.007797
2809085.00	0.009959
3134434.00	0.012076
4389300.00	0.022288
6088035.00	0.041907
7315605.00	0.061060
8290901.00	0.079963
9100972.00	0.098702
11798160.00	0.191055
13338220.00	0.282260
14301530.00	0.372894
14923620.00	0.463189
15326260.00	0.553267
15580470.00	0.643197
15730880.00	0.733025
15828890.00	0.912480
15828890.00	89.694270

Spring #27	
Depth: -19.50 m	
p [N/m]	y [m]
0.00	0.000000
743323.60	0.001156
1050693.00	0.001899
1484422.00	0.003212
2095108.00	0.005594
2560871.00	0.007839
2951172.00	0.010013
3292977.00	0.012140
4611316.00	0.022407
6395974.00	0.042133
7685636.00	0.061389
8710263.00	0.080393
9561309.00	0.099233
12394920.00	0.192082
14012880.00	0.283778
15024910.00	0.374899
15678470.00	0.465679
16101480.00	0.556241
16368550.00	0.646656
16526560.00	0.736966
16629530.00	0.917385
16629530.00	90.176490

Spring #28	
Depth: -20.25 m	
p [N/m]	y [m]
0.00	0.000000
778407.80	0.001162
1100285.00	0.001909
1554485.00	0.003229
2193995.00	0.005624
2681741.00	0.007881
3090464.00	0.010066
3448402.00	0.012205
4828965.00	0.022527
6697858.00	0.042358
8048390.00	0.061717
9121379.00	0.080823
10012590.00	0.099763
12979950.00	0.193109
14674270.00	0.285295
15734080.00	0.376903
16418480.00	0.468170
16861450.00	0.559216
17141130.00	0.650114
17306600.00	0.740907
17414430.00	0.922291
17414430.00	90.658720

Spring #29	
Depth: -21.00 m	
p [N/m]	y [m]
0.00	0.000000
807219.90	0.001163
1141011.00	0.001910
1612023.00	0.003232
2275203.00	0.005629
2781004.00	0.007888
3204855.00	0.010075
3576042.00	0.012216
5007706.00	0.022547
6945774.00	0.042396
8346295.00	0.061772
9458999.00	0.080894
10383200.00	0.099852
13460390.00	0.193280
15217430.00	0.285548
16316460.00	0.377238
17026200.00	0.468585
17485560.00	0.559712
17775590.00	0.650690
17947190.00	0.741564
18059010.00	0.923109
18059010.00	90.739090

Spring #30	
Depth: -21.75 m	
p [N/m]	y [m]
0.00	0.000000
836032.10	0.001290
1181737.00	0.002119
1669561.00	0.003585
2356412.00	0.006244
2880266.00	0.008750
3319246.00	0.011176
3703682.00	0.013551
5186446.00	0.025011
7193689.00	0.047028
8644199.00	0.068521
9796620.00	0.089733
10753810.00	0.110761
13940830.00	0.214398
15760580.00	0.316747
16898840.00	0.418454
17633920.00	0.519782
18109680.00	0.620866
18410060.00	0.721784
18587780.00	0.822587
18703590.00	1.023967
18703590.00	100.653200

Spring #31	
Depth: -22.50 m	
p [N/m]	y [m]
0.00	0.000000
864844.20	0.001361
1222463.00	0.002236
1727099.00	0.003782
2437621.00	0.006588
2979529.00	0.009232
3433637.00	0.011792
3831321.00	0.014298
5365186.00	0.026389
7441605.00	0.049620
8942104.00	0.072297
10134240.00	0.094678
11124420.00	0.116866
14421280.00	0.226214
16303740.00	0.334204
17481230.00	0.441516
18241630.00	0.548429
18733790.00	0.655083
19044520.00	0.761564
19228370.00	0.867922
19348170.00	1.080401
19348170.00	106.200500

Spring #32	
Depth: -23.25 m	
p [N/m]	y [m]
0.00	0.000000
893656.30	0.001378
1263190.00	0.002263
1784637.00	0.003829
2518830.00	0.006670
3078791.00	0.009346
3548028.00	0.011938
3958961.00	0.014474
5543926.00	0.026714
7689521.00	0.050231
9240009.00	0.073188
10471860.00	0.095846
11495030.00	0.118307
14901720.00	0.229003
16846900.00	0.338324
18063610.00	0.446960
18849350.00	0.555191
19357900.00	0.663160
19678990.00	0.770953
19868960.00	0.878623
19992750.00	1.093722
19992750.00	107.509900

Spring #33	
Depth: -24.00 m	
p [N/m]	y [m]
0.00	0.000000
922468.40	0.001429
1303916.00	0.002347
1842175.00	0.003971
2600039.00	0.006917
3178054.00	0.009693
3662419.00	0.012381
4086601.00	0.015011
5722666.00	0.027706
7937436.00	0.052096
9537913.00	0.075906
10809480.00	0.099404
11865630.00	0.122699
15382160.00	0.237506
17390050.00	0.350886
18646000.00	0.463555
19457070.00	0.575804
19982010.00	0.687783
20313450.00	0.799578
20509550.00	0.911246
20637330.00	1.134331
20637330.00	111.501700

Spring #34	
Depth: -24.75 m	
p [N/m]	y [m]
0.00	0.000000
951280.60	0.001471
1344642.00	0.002416
1899713.00	0.004088
2681248.00	0.007120
3277316.00	0.009977
3776810.00	0.012744
4214241.00	0.015451
5901407.00	0.028518
8185352.00	0.053624
9835818.00	0.078131
11147100.00	0.102318
12236240.00	0.126296
15862600.00	0.244468
17933210.00	0.361171
19228380.00	0.477144
20064780.00	0.592683
20606130.00	0.707944
20947920.00	0.823016
21150140.00	0.937957
21281920.00	1.167581
21281920.00	114.770100

Spring #35	
Depth: -25.50 m	
p [N/m]	y [m]
0.00	0.000000
980092.70	0.001801
1385368.00	0.002958
1957251.00	0.005004
2762457.00	0.008715
3376579.00	0.012213
3891201.00	0.015599
4341881.00	0.018914
6080147.00	0.034909
8433268.00	0.065640
10133720.00	0.095639
11484720.00	0.125247
12606850.00	0.154598
16343050.00	0.299250
18476360.00	0.442106
19810760.00	0.584067
20672500.00	0.725497
21230240.00	0.866586
21582380.00	1.007445
21790730.00	1.148143
21926500.00	1.429224
21926500.00	140.488900

Spring #36	
Depth: -26.25 m	
p [N/m]	y [m]
0.00	0.000000
1008905.00	0.001871
1426094.00	0.003073
2014789.00	0.005198
2843666.00	0.009055
3475841.00	0.012688
4005592.00	0.016206
4469520.00	0.019650
6258887.00	0.036267
8681184.00	0.068194
10431630.00	0.099360
11822340.00	0.130119
12977460.00	0.160612
16823490.00	0.310892
19019520.00	0.459305
20393150.00	0.606788
21280220.00	0.753720
21854350.00	0.900298
22216850.00	1.046637
22431320.00	1.192808
22571080.00	1.484823
22571080.00	145.954100

Spring #37	
Depth: -27.00 m	
p [N/m]	y [m]
0.00	0.000000
1037717.00	0.001885
1466820.00	0.003095
2072327.00	0.005236
2924875.00	0.009121
3575104.00	0.012782
4119983.00	0.016325
4597160.00	0.019794
6437627.00	0.036533
8929099.00	0.068694
10729530.00	0.100089
12159960.00	0.131074
13348070.00	0.161791
17303930.00	0.313174
19562680.00	0.462677
20975530.00	0.611243
21887930.00	0.759254
22478460.00	0.906908
22851310.00	1.054321
23071910.00	1.201566
23215660.00	1.495725
23215660.00	147.025700

Spring #38	
Depth: -27.75 m	
p [N/m]	y [m]
0.00	0.000000
1066529.00	0.001885
1507546.00	0.003095
2129865.00	0.005236
3006084.00	0.009121
3674366.00	0.012782
4234374.00	0.016325
4724800.00	0.019794
6616367.00	0.036533
9177015.00	0.068694
11027440.00	0.100089
12497580.00	0.131074
13718670.00	0.161791
17784370.00	0.313174
20105830.00	0.462677
21557910.00	0.611243
22495650.00	0.759254
23102580.00	0.906908
23485770.00	1.054321
23712500.00	1.201566
23860240.00	1.495725
23860240.00	147.025700

Spring #39	
Depth: -28.50 m	
p [N/m]	y [m]
0.00	0.000000
1095341.00	0.001846
1548273.00	0.003032
2187403.00	0.005129
3087293.00	0.008935
3773629.00	0.012521
4348765.00	0.015992
4852440.00	0.019390
6795108.00	0.035788
9424931.00	0.067292
11325340.00	0.098047
12835200.00	0.128399
14089280.00	0.158489
18264810.00	0.306783
20648990.00	0.453235
22140300.00	0.598768
23103370.00	0.743759
23726690.00	0.888400
24120240.00	1.032805
24353090.00	1.177044
24504820.00	1.465200
24504820.00	144.025200

Spring #40	
Depth: -29.25 m	
p [N/m]	y [m]
0.00	0.000000
1124153.00	0.001846
1588999.00	0.003032
2244941.00	0.005129
3168502.00	0.008935
3872891.00	0.012521
4463156.00	0.015992
4980079.00	0.019390
6973848.00	0.035788
9672847.00	0.067292
11623250.00	0.098047
13172820.00	0.128399
14459890.00	0.158489
18745260.00	0.306783
21192150.00	0.453235
22722680.00	0.598768
23711080.00	0.743759
24350800.00	0.888400
24754700.00	1.032805
24993680.00	1.177044
25149400.00	1.465200
25149400.00	144.025200

Spring #41	
Depth: -30.00 m	
p [N/m]	y [m]
0.00	0.000000
1152965.00	0.001846
1629725.00	0.003032
2302479.00	0.005129
3249710.00	0.008935
3972154.00	0.012521
4577547.00	0.015992
5107719.00	0.019390
7152588.00	0.035788
9920762.00	0.067292
11921150.00	0.098047
13510440.00	0.128399
14830500.00	0.158489
19225700.00	0.306783
21735300.00	0.453235
23305070.00	0.598768
24318800.00	0.743759
24974920.00	0.888400
25389170.00	1.032805
25634270.00	1.177044
25793980.00	1.465200
25793980.00	144.025200

Spring #42	
Depth: -30.75 m	
p [N/m]	y [m]
0.00	0.000000
1181778.00	0.001846
1670451.00	0.003032
2360017.00	0.005129
3330919.00	0.008935
4071416.00	0.012521
4691938.00	0.015992
5235359.00	0.019390
7331328.00	0.035788
10168680.00	0.067292
12219050.00	0.098047
13848060.00	0.128399
15201100.00	0.158489
19706140.00	0.306783
22278460.00	0.453235
23887450.00	0.598768
24926520.00	0.743759
25599030.00	0.888400
26023630.00	1.032805
26274860.00	1.177044
26438560.00	1.465200
26438560.00	144.025200

Spring #43	
Depth: -31.50 m	
p [N/m]	y [m]
0.00	0.000000
1210590.00	0.001846
1711177.00	0.003032
2417555.00	0.005129
3412128.00	0.008935
4170679.00	0.012521
4806329.00	0.015992
5362999.00	0.019390
7510068.00	0.035788
10416590.00	0.067292
12516960.00	0.098047
14185680.00	0.128399
15571710.00	0.158489
20186580.00	0.306783
22821610.00	0.453235
24469830.00	0.598768
25534230.00	0.743759
26223140.00	0.888400
26658100.00	1.032805
26915440.00	1.177044
27083140.00	1.465200
27083140.00	144.025200

Spring #44	
Depth: -32.25 m	
p [N/m]	y [m]
0.00	0.000000
1239402.00	0.001846
1751903.00	0.003032
2475093.00	0.005129
3493337.00	0.008935
4269941.00	0.012521
4920720.00	0.015992
5490639.00	0.019390
7688809.00	0.035788
10664510.00	0.067292
12814860.00	0.098047
14523310.00	0.128399
15942320.00	0.158489
20667030.00	0.306783
23364770.00	0.453235
25052220.00	0.598768
26141950.00	0.743759
26847250.00	0.888400
27292560.00	1.032805
27556030.00	1.177044
27727720.00	1.465200
27727720.00	144.025200

Spring #45	
Depth: -33.00 m	
p [N/m]	y [m]
0.00	0.000000
1268214.00	0.001846
1792630.00	0.003032
2532631.00	0.005129
3574546.00	0.008935
4369203.00	0.012521
5035111.00	0.015992
5618278.00	0.019390
7867549.00	0.035788
10912430.00	0.067292
13112770.00	0.098047
14860930.00	0.128399
16312930.00	0.158489
21147470.00	0.306783
23907930.00	0.453235
25634600.00	0.598768
26749670.00	0.743759
27471370.00	0.888400
27927030.00	1.032805
28196620.00	1.177044
28372310.00	1.465200
28372310.00	144.025200

Spring #46	
Depth: -33.75 m	
p [N/m]	y [m]
0.00	0.000000
1297026.00	0.001846
1833356.00	0.003032
2590169.00	0.005129
3655755.00	0.008935
4468466.00	0.012521
5149502.00	0.015992
5745918.00	0.019390
8046289.00	0.035788
11160340.00	0.067292
13410670.00	0.098047
15198550.00	0.128399
16683540.00	0.158489
21627910.00	0.306783
24451080.00	0.453235
26216990.00	0.598768
27357380.00	0.743759
28095480.00	0.888400
28561490.00	1.032805
28837210.00	1.177044
29016890.00	1.465200
29016890.00	144.025200

Spring #47	
Depth: -34.50 m	
p [N/m]	y [m]
0.00	0.000000
1325838.00	0.001846
1874082.00	0.003032
2647707.00	0.005129
3736964.00	0.008935
4567728.00	0.012521
5263893.00	0.015992
5873558.00	0.019390
8225029.00	0.035788
11408260.00	0.067292
13708580.00	0.098047
15536170.00	0.128399
17054140.00	0.158489
22108350.00	0.306783
24994240.00	0.453235
26799370.00	0.598768
27965100.00	0.743759
28719590.00	0.888400
29195960.00	1.032805
29477800.00	1.177044
29661470.00	1.465200
29661470.00	144.025200

Spring #48	
Depth: -35.25 m	
p [N/m]	y [m]
0.00	0.000000
1354650.00	0.001846
1914808.00	0.003032
2705245.00	0.005129
3818173.00	0.008935
4666991.00	0.012521
5378284.00	0.015992
6001198.00	0.019390
8403770.00	0.035788
11656170.00	0.067292
14006480.00	0.098047
15873790.00	0.128399
17424750.00	0.158489
22588790.00	0.306783
25537390.00	0.453235
27381750.00	0.598768
28572820.00	0.743759
29343710.00	0.888400
29830420.00	1.032805
30118390.00	1.177044
30306050.00	1.465200
30306050.00	144.025200

Spring #49	
Depth: -36.00 m	
p [N/m]	y [m]
0.00	0.000000
1383462.00	0.001846
1955534.00	0.003032
2762783.00	0.005129
3899382.00	0.008935
4766253.00	0.012521
5492675.00	0.015992
6128837.00	0.019390
8582510.00	0.035788
11904090.00	0.067292
14304390.00	0.098047
16211410.00	0.128399
17795360.00	0.158489
23069240.00	0.306783
26080550.00	0.453235
27964140.00	0.598768
29180530.00	0.743759
29967820.00	0.888400
30464890.00	1.032805
30758980.00	1.177044
30950630.00	1.465200
30950630.00	144.025200

Spring #50	
Depth: -36.75 m	
p [N/m]	y [m]
0.00	0.000000
1412275.00	0.001846
1996260.00	0.003032
2820321.00	0.005129
3980591.00	0.008935
4865516.00	0.012521
5607066.00	0.015992
6256477.00	0.019390
8761250.00	0.035788
12152000.00	0.067292
14602290.00	0.098047
16549030.00	0.128399
18165970.00	0.158489
23549680.00	0.306783
26623710.00	0.453235
28546520.00	0.598768
29788250.00	0.743759
30591930.00	0.888400
31099350.00	1.032805
31399570.00	1.177044
31595210.00	1.465200
31595210.00	144.025200

Spring #51	
Depth: -37.50 m	
p [N/m]	y [m]
0.00	0.000000
1441087.00	0.001846
2036986.00	0.003032
2877859.00	0.005129
4061800.00	0.008935
4964778.00	0.012521
5721457.00	0.015992
6384117.00	0.019390
8939990.00	0.035788
12399920.00	0.067292
14900200.00	0.098047
16886650.00	0.128399
18536580.00	0.158489
24030120.00	0.306783
27166860.00	0.453235
29128910.00	0.598768
30395970.00	0.743759
31216040.00	0.888400
31733820.00	1.032805
32040160.00	1.177044
32239790.00	1.465200
32239790.00	144.025200

Spring #52	
Depth: -38.25 m	
p [N/m]	y [m]
0.00	0.000000
1469899.00	0.001846
2077713.00	0.003032
2935397.00	0.005129
4143009.00	0.008935
5064041.00	0.012521
5835848.00	0.015992
6511757.00	0.019390
9118730.00	0.035788
12647840.00	0.067292
15198100.00	0.098047
17224270.00	0.128399
18907180.00	0.158489
24510560.00	0.306783
27710020.00	0.453235
29711290.00	0.598768
31003680.00	0.743759
31840160.00	0.888400
32368280.00	1.032805
32680750.00	1.177044
32884370.00	1.465200
32884370.00	144.025200

Spring #53	
Depth: -39.00 m	
p [N/m]	y [m]
0.00	0.000000
1498711.00	0.001846
2118439.00	0.003032
2992935.00	0.005129
4224217.00	0.008935
5163303.00	0.012521
5950239.00	0.015992
6639397.00	0.019390
9297471.00	0.035788
12895750.00	0.067292
15496000.00	0.098047
17561890.00	0.128399
19277790.00	0.158489
24991010.00	0.306783
28253180.00	0.453235
30293670.00	0.598768
31611400.00	0.743759
32464270.00	0.888400
33002750.00	1.032805
33321340.00	1.177044
33528950.00	1.465200
33528950.00	144.025200

Spring #54	
Depth: -39.75 m	
p [N/m]	y [m]
0.00	0.000000
1527523.00	0.001846
2159165.00	0.003032
3050473.00	0.005129
4305426.00	0.008935
5262566.00	0.012521
6064631.00	0.015992
6767036.00	0.019390
9476211.00	0.035788
13143670.00	0.067292
15793910.00	0.098047
17899510.00	0.128399
19648400.00	0.158489
25471450.00	0.306783
28796330.00	0.453235
30876060.00	0.598768
32219120.00	0.743759
33088380.00	0.888400
33637210.00	1.032805
33961930.00	1.177044
34173530.00	1.465200
34173530.00	144.025200

Spring #55	
Depth: -40.50 m	
p [N/m]	y [m]
0.00	0.000000
1556335.00	0.001846
2199891.00	0.003032
3108011.00	0.005129
4386635.00	0.008935
5361828.00	0.012521
6179022.00	0.015992
6894676.00	0.019390
9654951.00	0.035788
13391580.00	0.067292
16091810.00	0.098047
18237130.00	0.128399
20019010.00	0.158489
25951890.00	0.306783
29339490.00	0.453235
31458440.00	0.598768
32826830.00	0.743759
33712490.00	0.888400
34271680.00	1.032805
34602520.00	1.177044
34818110.00	1.465200
34818110.00	144.025200

Spring #56	
Depth: -41.25 m	
p [N/m]	y [m]
0.00	0.000000
1585147.00	0.001846
2240617.00	0.003032
3165549.00	0.005129
4467844.00	0.008935
5461091.00	0.012521
6293413.00	0.015992
7022316.00	0.019390
9833691.00	0.035788
13639500.00	0.067292
16389720.00	0.098047
18574750.00	0.128399
20389620.00	0.158489
26432330.00	0.306783
29882640.00	0.453235
32040830.00	0.598768
33434550.00	0.743759
34336610.00	0.888400
34906140.00	1.032805
35243110.00	1.177044
35462700.00	1.465200
35462700.00	144.025200

Spring #57	
Depth: -42.00 m	
p [N/m]	y [m]
0.00	0.000000
1613960.00	0.001846
2281343.00	0.003032
3223087.00	0.005129
4549053.00	0.008935
5560353.00	0.012521
6407804.00	0.015992
7149956.00	0.019390
10012430.00	0.035788
13887410.00	0.067292
16687620.00	0.098047
18912370.00	0.128399
20760220.00	0.158489
26912770.00	0.306783
30425800.00	0.453235
32623210.00	0.598768
34042270.00	0.743759
34960720.00	0.888400
35540610.00	1.032805
35883700.00	1.177044
36107280.00	1.465200
36107280.00	144.025200

Spring #58	
Depth: -42.75 m	
p [N/m]	y [m]
0.00	0.000000
1642772.00	0.001846
2322069.00	0.003032
3280625.00	0.005129
4630262.00	0.008935
5659616.00	0.012521
6522195.00	0.015992
7277596.00	0.019390
10191170.00	0.035788
14135330.00	0.067292
16985530.00	0.098047
19249990.00	0.128399
21130830.00	0.158489
27393220.00	0.306783
30968960.00	0.453235
33205590.00	0.598768
34649980.00	0.743759
35584830.00	0.888400
36175070.00	1.032805
36524290.00	1.177044
36751860.00	1.465200
36751860.00	144.025200

Spring #59	
Depth: -43.50 m	
p [N/m]	y [m]
0.00	0.000000
1671584.00	0.001846
2362796.00	0.003032
3338163.00	0.005129
4711471.00	0.008935
5758878.00	0.012521
6636586.00	0.015992
7405235.00	0.019390
10369910.00	0.035788
14383250.00	0.067292
17283430.00	0.098047
19587610.00	0.128399
21501440.00	0.158489
27873660.00	0.306783
31512110.00	0.453235
33787980.00	0.598768
35257700.00	0.743759
36208950.00	0.888400
36809540.00	1.032805
37164880.00	1.177044
37396440.00	1.465200
37396440.00	144.025200

Spring #60	
Depth: -44.25 m	
p [N/m]	y [m]
0.00	0.000000
1700396.00	0.001846
2403522.00	0.003032
3395701.00	0.005129
4792680.00	0.008935
5858140.00	0.012521
6750977.00	0.015992
7532875.00	0.019390
10548650.00	0.035788
14631160.00	0.067292
17581340.00	0.098047
19925230.00	0.128399
21872050.00	0.158489
28354100.00	0.306783
32055270.00	0.453235
34370360.00	0.598768
35865420.00	0.743759
36833060.00	0.888400
37444000.00	1.032805
37805470.00	1.177044
38041020.00	1.465200
38041020.00	144.025200

Spring #61	
Depth: -45.00 m	
p [N/m]	y [m]
0.00	0.000000
1729208.00	0.001846
2444248.00	0.003032
3453239.00	0.005129
4873889.00	0.008935
5957403.00	0.012521
6865368.00	0.015992
7660515.00	0.019390
10727390.00	0.035788
14879080.00	0.067292
17879240.00	0.098047
20262850.00	0.128399
22242660.00	0.158489
28834540.00	0.306783
32598420.00	0.453235
34952750.00	0.598768
36473130.00	0.743759
37457170.00	0.888400
38078460.00	1.032805
38446060.00	1.177044
38685600.00	1.465200
38685600.00	144.025200

Appendix C. Soil-Structure Interaction Damping

The REDWIN macro-element model accounts for a hysteretic damping. This damping is characterized internally by the REDWIN macro-element model based on the nonlinear load-deflection curves provided by the user as input.

In this section, the SSI damping is characterized at different loading levels in order to inform other proposed SSI methods in this report (e.g., apparent fixity, coupled springs, and distributed springs).

The SSI damping can be quantified by means of a free-decay test comparing the response of the system when using the REDWIN macro-element model and the response of the system when using a stiffness matrix at the seabed (see Figure C-1). The REDWIN macro-element model dissipates energy at the foundation while the elastic stiffness matrix approach does not. The boundary conditions are the same as the ones used in LC 2.3 with the only difference being that the initial loading for this free-decay test is a horizontal force of 1,875 kN at the yaw bearing. Note that this force is 25% higher than the thrust force at rated wind speed for the studied wind turbine (Bortolotti et al. 2019) and therefore it allows characterization of the damping for a wide range of loading levels. The decay response observed in Figure C-1 accounts for the structural damping of the tower and monopile, the SSI damping (REDWIN model only), and the hydrodynamic damping from the still water due to the viscous-drag component in the Morison equation.

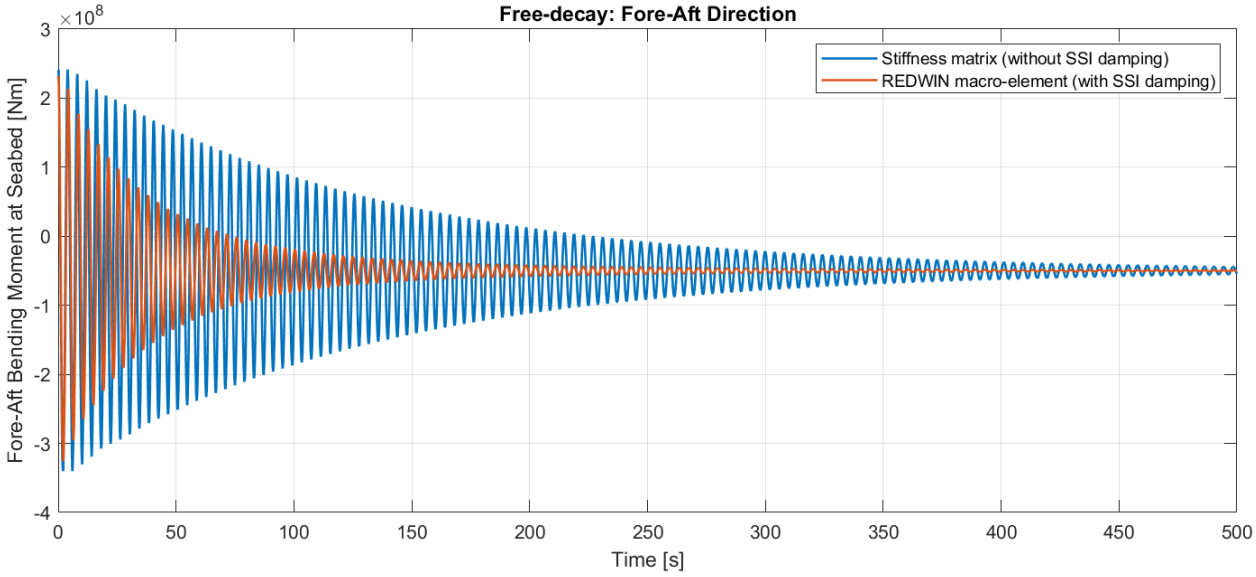

Figure C-1. Free-decay test for the REDWIN macro-element model and the equivalent elastic stiffness matrix at the seabed

From the free-decay test observed in Figure C-1, it is possible to calculate the damping ratio by means of the logarithmic decrement approach. The logarithmic decrement (δ) can be determined by the difference in amplitude for *n* given peaks (see Figure C-2 and Eq. C-1).

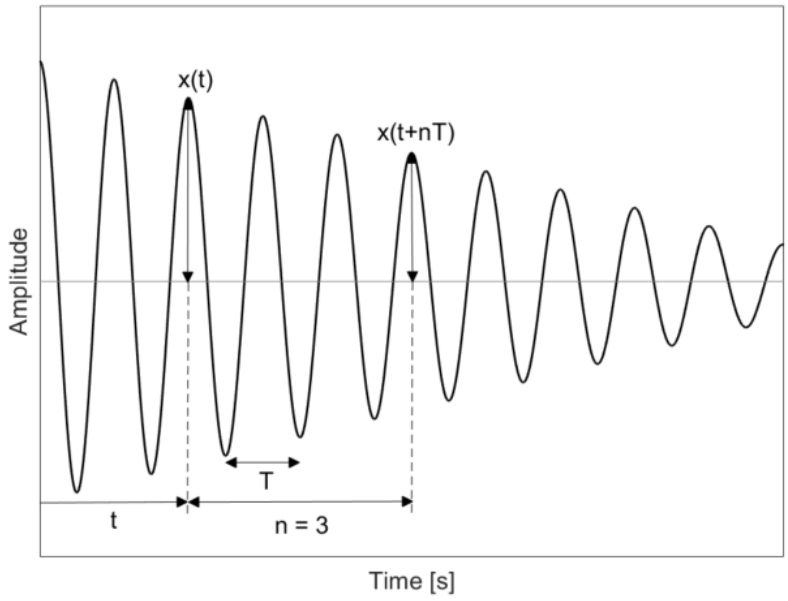

Figure C-2. Illustrative plot of a free-decay test and the relationship between the amplitude at instant t and 3 periods away (n = 3)

$$\delta = \frac{1}{n} ln \frac{x(t)}{x(t+nT)} \qquad \text{(C-1)}$$

Where *x(t)* is the amplitude at time *t* and *x(t + nT)* is the amplitude of the peak *n* periods (*T*) away (being *n* a positive integer number).

Once the logarithmic decrement is known, the damping ratio (ζ) can be calculated according to Eq. C-2.

$$\zeta = \frac{\delta}{\sqrt{(2\pi)^2 + \delta^2}} \qquad \text{(C-2)}$$

This approach has been used to calculate the damping ratios from a single free decay (see Figure C-1) at five different loading levels corresponding to amplitudes equivalent to rated thrust force, 75% of rated thrust, 50% of rated thrust, 25% of rated thrust, and idling. Figure C-3 shows the corresponding damping ratios for the system when accounting and not accounting for the energy dissipated due to the soil-structure interaction. The damping ratios shown in Figure C-3 have been calculated based on the average results of three successive cycles (accounting for peaks and troughs) around the corresponding amplitude of interest.

As it can be observed in Figure C-3, the damping for the REDWIN macro-element approach for large amplitudes (e.g., between amplitudes equivalent to the rated thrust and 25% of the rated thrust) is significantly larger than for the system without soil-structure interaction damping. It can also be observed that the nonlinear nature of the damping for the REDWIN macro-element approach creates larger damping at larger amplitudes. On the other hand, the approach that uses the stiffness matrix without accounting for the energy dissipated by the soil-structure interaction is relatively constant, and very close to the structural damping defined for the tower and monopile (0.50% critical damping).

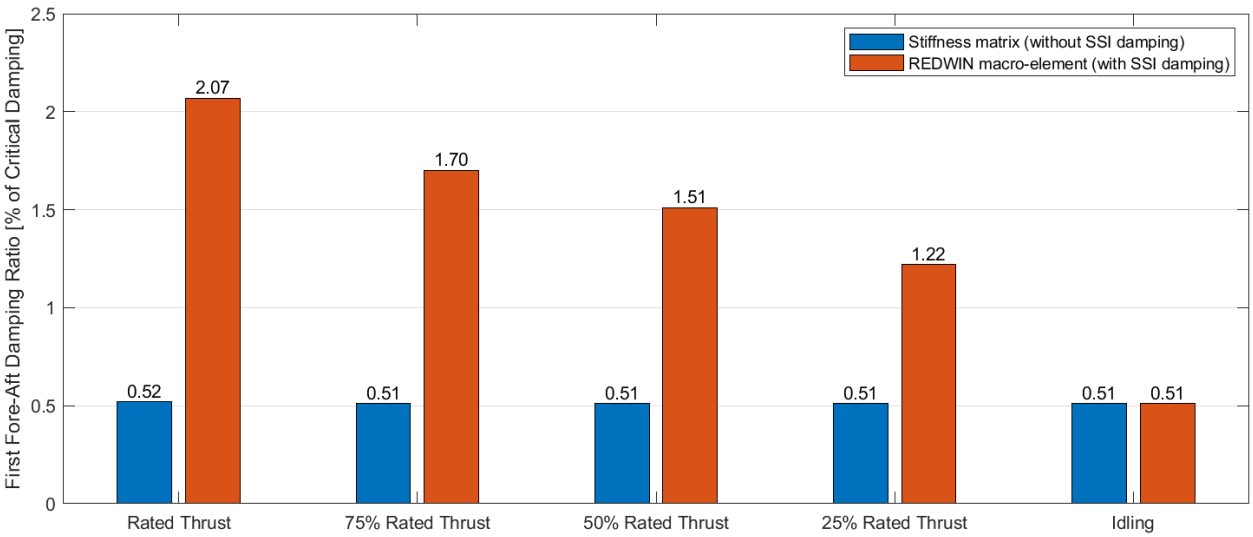

Figure C-3. Global damping ratio for the first fore-aft bending mode for the REDWIN macro-element model and the equivalent elastic stiffness matrix at the seabed

It is important to note that the models analyzed in OC6 Phase II do not account for aerodynamic damping. Therefore, the resultant damping values observed in Figure C-3 are due to contributions in terms of structure, hydro, and soil-structure interaction (for the REDWIN macro-element approach). Additionally, the derived damping values assume zero mean thrust load. The actual damping from the REDWIN macro-element approach may differ if nonzero mean thrust loads are applied.

Figure C-4 shows the force-displacement and bending-rotation relationships at the seabed location. These load-deflection curves correspond to the response of the system from t = 10 s to t = 300 s during the free-decay test shown in Figure C-1. As it can be observed, the cuves are not centered at zero in terms of loads and deflections because the system oscillates around the static equilibrium solution. The static equilibrium is determined by the gravity load and the compliance at the seabed. The eccentric mass of the RNA (see Table 6 for reference) creates the offset in terms of displacements in the *x* direction and the rotation around the *y* axis.

It can also be observed that the stiffness matrix approach does not pass through the zero load and zero deflection at any instant. The reason for this is the coupling between the horizontal and rotational directions. For example, the displacement would be zero for a zero force only if the corresponding bending moment was also zero. A similar behavior can be observed for the REDWIN macro-element approach. But in this case the deflections are even farther from zero due to the elasto-plastic behavior.

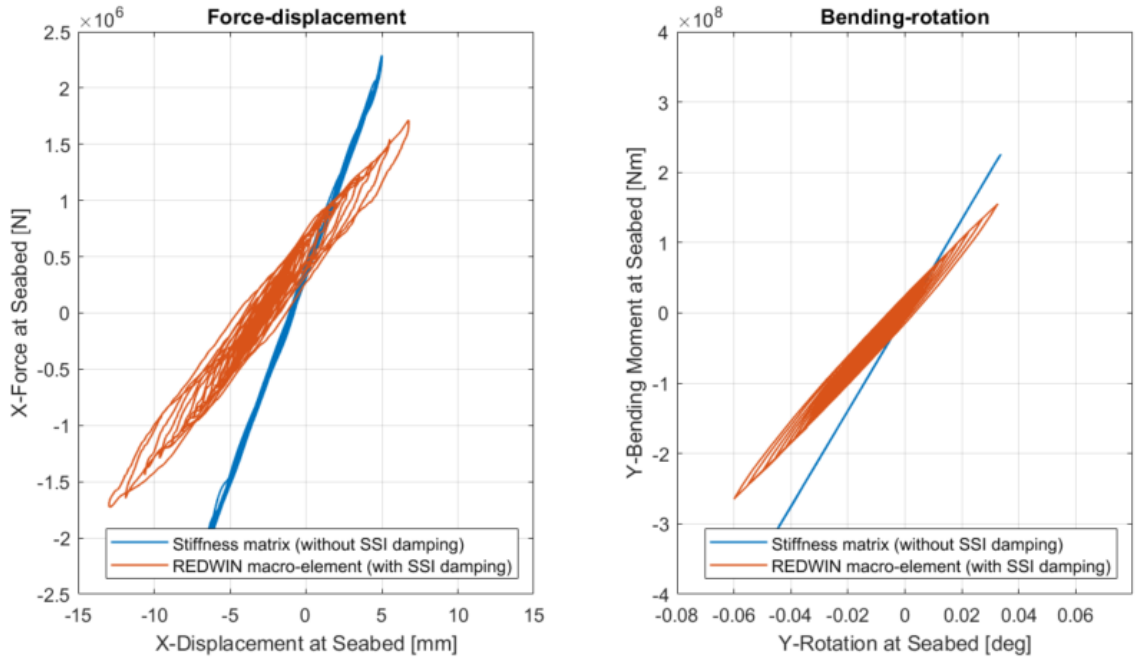

Figure C-4. Force-displacement (left) and bending-rotation (right) relationships for the free-decay test at the seabed location

In Figure C-4, the nonlinear behavior of the REDWIN macro-element and the linear nature of the elastic stiffness matrix can be clearly observed. For large amplitudes, the stiffness of the REDWIN macro-element becomes softer than the one prescribed in the stiffness matrix approach and only for small amplitudes both stiffness are equivalent (see Figure C-5 for reference).

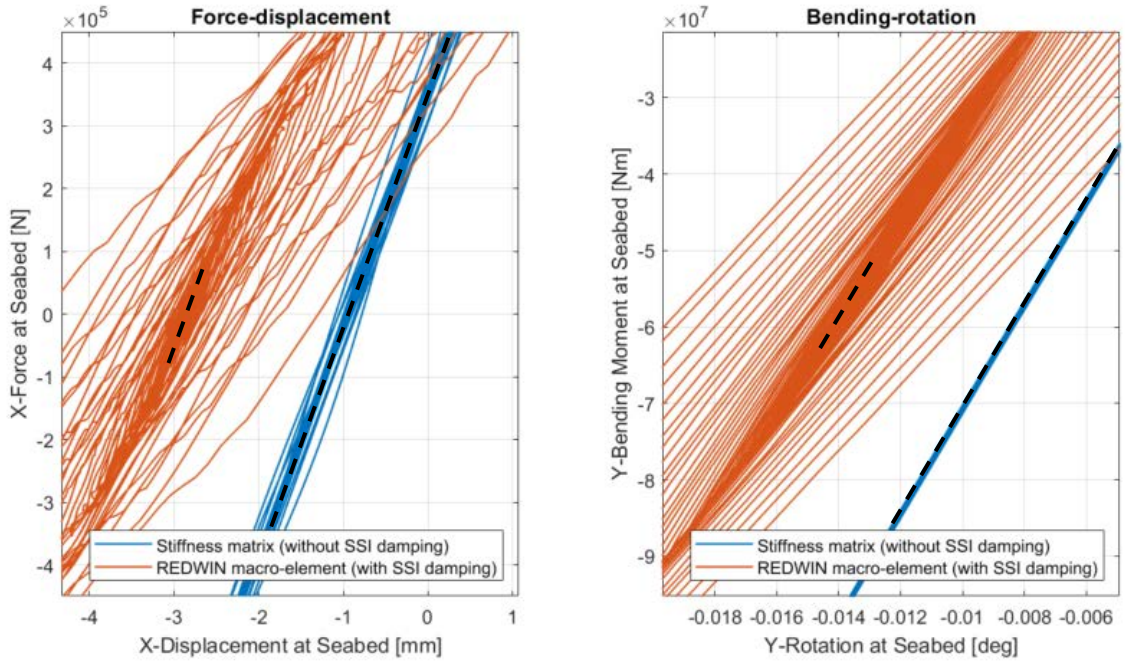

Figure C-5. Zoom-in of Figure C-4 with the equivalent stiffness denoted with a dashed black line for the force-displacement (left) and bending-rotation (right) relationships at the seabed

It is also interesting to note that the area contained in the load-deflection hysteresis loops at the seabed is equivalent to the energy dissipated by the soil-structure interaction. As it can be observed in Figure C-4 and Figure C-5, the REDWIN macro-element provides damping to the system while the stiffness matrix does not. Moreover, the energy dissipated by the REDWIN macro-element approach depends on the amplitude. The area of the hysteresis loop is large when the system undergoes large amplitudes, and it is almost null when the amplitudes are small. This is aligned with the results obtained in Figure C-3. In addition, it can be observed that the approach that uses the stiffness matrix approach (blue curve in Figure C-4 and Figure C-5) follows the same path during the loading and unloading conditions. This denotes the elastic nature of the foundation model and confirms that the system does not dissipate energy due to the the soil-structure interaction.

Finally, it is important to realize that the results presented in Appendix C are representative of the system studied in OC6 Phase II. The energy dissipated by the soil-structure interaction depends on the soil properties and the compliance of the foundation. For example, if the foundation is very stiff compared to the supporting structure, the amplitudes at the foundation level would be relatively small and the damping contribution from the soil-structure interaction would not play a significant role in the overall system.

Appendix D. Externally Applied Loads

OC6 Phase II focused on the verification of the soil-structure interaction model. To avoid the differences coming from the aerodynamic models, the loads at the yaw bearing were prescribed.

LC 3.1 considers a mean wind speed at hub height of 9.06 m/s. This wind speed is below the rated wind speed (10.75 m/s) of the IEA-10.0-198-RWT. Figure D-1 shows the probability density function (PDF) of the rotor speed simulated in OpenFAST for this load case.

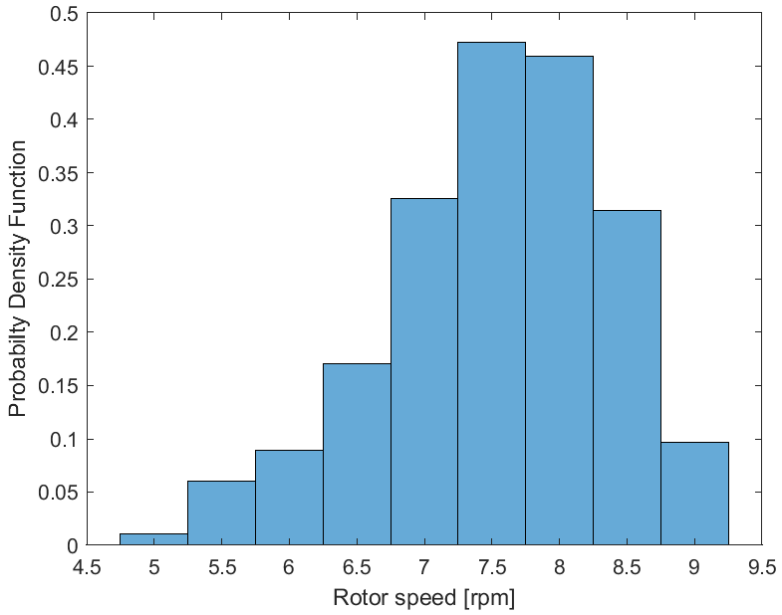

Figure D-1. Probability density function of rotor speed in LC 3.1

As can be observed in the PDF, the wind turbine is rotating most of the time around 7.75 rpm. The aeroelastic model considered in OpenFAST does not include any rotor imbalance (e.g., pitch imbalance or blade mass imbalance). Accordingly, it is expected that the excitations present in the computed loads correspond to the blade passing frequency (3P for a three-bladed wind turbine) and the corresponding harmonics, where P is the rotor speed.

Table D-1. Main Excitations in the Externally Applied Loads for LC 3.1

Description	Acronym	Frequency [Hz]
Fundamental frequency	3P	0.388
Second harmonic	6P	0.775
Third harmonic	9P	1.163

Figure D-2 shows the power spectral density (PSD) of the force in the fore-aft direction at the yaw bearing. The PSD plots shown in Figure D-2 and Figure D-4 use a frequency resolution of 0.01 Hz, 50% overlapping, and Hanning window. The main excitations observed in the spectrum correspond to 3P, 6P, and 9P.

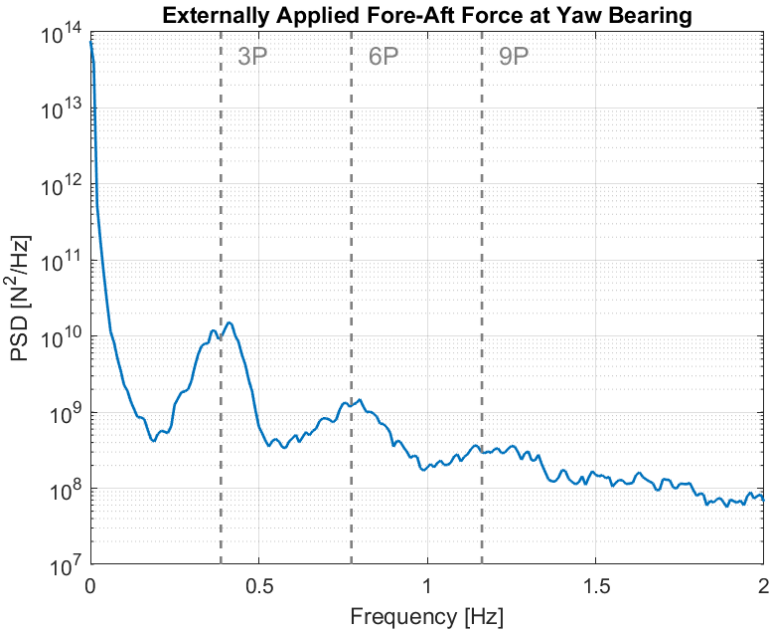

Figure D-2. Power spectral density of the fore-aft force at the yaw bearing for LC 3.1

LC 3.2 examines the system response for a mean hub height wind speed of 20.90 m/s. In this case, the rotor is rotating at rated speed (8.68 rpm). Figure D-3 shows the PDF of the rotor speed for this load case.

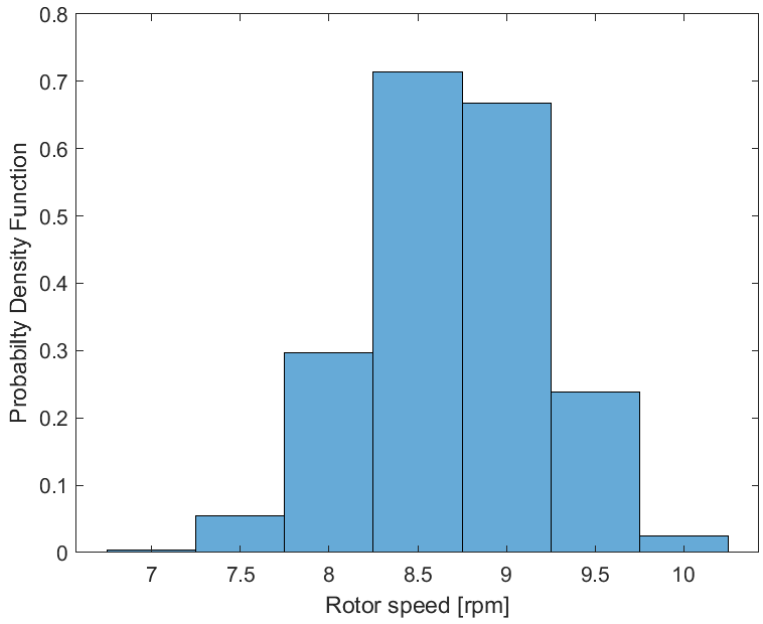

Figure D-3. Probability density function of rotor speed in LC 3.2

As can be observed, in this case the rotor speed variations are smaller than for LC 3.1. The main reason is that for this wind condition, the wind turbine is operating well above the rated wind speed and the blade pitch control can maintain the wind turbine working close to the rotor rated speed.

Table D-2 shows the main excitations in the system for the LC 3.2.

Table D-2. Main Excitations in the Externally Applied Loads for LC 3.2

Description	Acronym	Frequency [Hz]
Fundamental frequency	3P	0.434
Second harmonic	6P	0.868
Third harmonic	9P	1.302

Compared to LC 3.1, the excitation frequencies are slightly higher (+12%).

Figure D-4 shows the PSD of the force in the fore-aft direction at the yaw bearing.

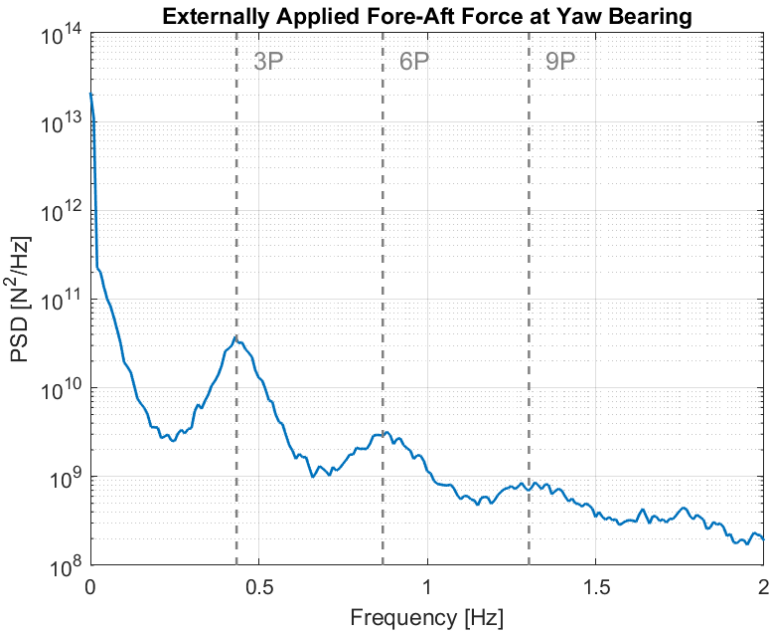

Figure D-4. Power spectral density of the fore-aft force at the yaw bearing for LC 3.2

Figure D-5 compares the PSD from LC 3.1 and LC 3.2. As expected, the higher average wind speed in LC 3.2 results in higher dynamic loads. It can also be observed that the amplitude at 0 Hz for LC 3.1 is larger than for LC 3.2. This indicates that the average fore-aft force at the yaw bearing in LC 3.1 is higher than for LC 3.2. In LC 3.1 the rotor thrust is close to its maximum because the wind turbine is just below the rated wind speed, while in the LC 3.2 the wind turbine is operating well above the rated wind speed with the blades pitched to keep the rotational speed under control.

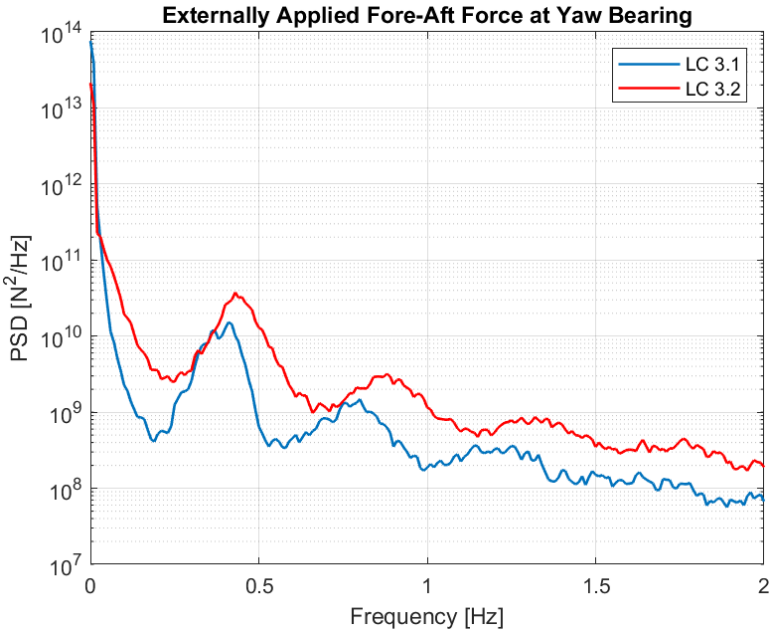

Figure D-5. Comparison of the power spectral density of the fore-aft force at the yaw bearing between LC 3.1 and LC 3.2